Rad52 mediates class-switch DNA recombination to IgD

Yijang Xu[1], Hang Zhou[1], Ginell Post[2], Hong Zan[1] and Paolo Casali[1,3]✉

[1]Department of Microbiology, Immunology & Molecular Genetics, University of Texas Long School of Medicine,
[2]Department of Pathology, University of Arkansas School of Medicine, Little Rock, AR 72205, USA.
[3]Department of Medicine, University of Texas Long School of Medicine, UT Health Science Center, San Antonio, TX 78229, USA. YX and HZ contributed equally to this work. ✉pcasali@uthscsa.edu

While the biology of IgD begins to be better understood, the mechanism of expression of this phylogenetically old and highly conserved Ig class remains unknown. In B cells, IgD is expressed together with IgM as transmembrane receptor for antigen through alternative splicing of long primary *V_HDJ_H-Cμ-s-m-Cδ-s-m* RNA, which also underpins the secreted form of IgD. IgD is also expressed through class switch DNA recombination (CSR), as initiated by AID-mediated double-strand DNA breaks (DSBs) in Sμ and σδ, and resolution of such DSBs by a yet unknown alternative endjoining (A-EJ) mechanism. This synapses Sμ with σδ region DSB resected ends leading to insertion of extensive S-S junction microhomologies, unlike the Ku70/Ku86-dependent NHEJ which resolves DSB blunt ends in CSR to IgG, IgA and IgE with little or no microhomologies. We previously demonstrated a novel role of DNA annealing homologous recombination Rad52 protein in "short-range" microhomology-mediated synapsis of intra-Sμ region DSBs. This led us to hypothesize that Rad52 is also involved in the short-range microhomology-mediated A-EJ recombination of Sμ with σδ,. We found that induction of IgD CSR by T-dependent or T-independent stimuli downregulated Zfp318 (the suppressor of *Cμ-s-m* transcription termination), promoted Rad52 phosphorylation, recruitment of Rad52 to Sμ and σδ, leading to Sμ-σδ recombination with extensive microhomologies, *V_HDJ_H-Cδs* transcription and sustained IgD secretion. Rad52 ablation in mouse *Rad52*$^{-/-}$ B cells aborted IgD CSR *in vitro* and *in vivo* and dampened the specific IgD antibody response to OVA. Further, Rad52 knockdown in human B cells virtually abrogated IgD CSR. Finally, Rad52 phosphorylation was associated with high levels IgD CSR and anti-nuclear IgD autoantibodies in lupus-prone mice and lupus patients. Thus, Rad52 mediates CSR to IgD by synapsing Sμ-σδ resected DSB ends through microhomology-mediated A-EJ and in concert with Zfp318 modulation. This is a previously unrecognized, critical and dedicated role of Rad52 in mammalian DNA repair.

IgD has been an enigmatic antibody class for many years, despite being evolutionarily ancient and highly conserved across species[1-6]. As primordial as IgM, IgD appeared in cartilaginous fishes, amphibians and occurs in fishes, rodents, cattle and humans[2,7]. As an example, in *Xenopus*, the Igδ exon cluster is in the same position, immediately 3′ of the Igμ locus, as it exists in mammals[7]. In mice and humans, IgD is expressed primarily as a transmembrane IgD receptor together with IgM with identical antigen specificity on naïve mature B cells in the form of BCR. IgD also exists as a secreted antibody. In humans, circulating IgD occurs at concentrations up to more than two-thousand folds greater than IgE (10-250 μg/ml vs. ~0.1 μg/ml), the rarest peripheral blood Ig class. IgD are secreted by $IgM^{-}IgD^{+}$ plasmablasts and plasma cells differentiated from B cells in lymphoepithelial organs in aerodigestive mucosae, including palatine and pharyngeal tonsils. $IgM^{-}IgD^{+}$B cells and plasma cells can also be found in the lachrymal, salivary and mammary glands[3]. In addition to existing as free molecule, IgD can occurs on the surface of innate effector cells, including basophils, mast cells and monocytes[1,8,9]. IgD bound to these cells would enhance immune surveillance and exert proinflammatory and antimicrobial effects[1,8,9]. These include triggering basophils to secret IL-4, IL-5 and IL-13 upon antigen engagement or attenuating basophil or mast cell allergic degranulation induced by IgE co-engagement[1]. Thus, IgD would contribute to mucosal homeostasis by endowing effector cells with reactivity to microbial commensals and pathogens[5,6].

Identifying the stimuli and molecular mechanisms that underpin IgD expression is important to understand the regulation of IgD secretion throughout the body. The immediately proximal location and unique integration of Cδ and Cμ gene loci in the same transcriptional unit allow these two Ig isotypes to be coordinately regulated in transcription[10,11]. In naive mature B cells, (membrane) mIgM and mIgD are co-expressed by alternative splicing of long primary transcripts consisting of rearranged V_HDJ_H exons and downstream Cμ and Cδ exons (V_HDJ_H-*Cμ-s-m-Cδ-s-m*). Alternative splicing of the same long primary V_HDJ_H-*Cμ-s-m-Cδ-s-m* RNA transcripts also leads to expression of (secreted) sIgM and sIgD[2,8]. Transcription of long primary V_HDJ_H-*Cμ-s-m-Cδ-s-m* RNA requires the zinc finger ZFP318 repressor of transcriptional termination, which obliterates the effect of the transcriptional termination sites (TTS) intercalated between the Cμ and Cδ exon clusters[10,11] (Fig. 1a). IgD can also be expressed through class switch DNA recombination (CSR), by which $IgM^{+}IgD^{+}$B cells juxtapose V_HDJ_H DNA from the Cμ (IgM) to the Cδ (IgD) exons cluster, giving rise to V_HDJ_H-*Cδm* RNA transcripts and $IgM^{-}IgD^{+}$B cells[1,5,8,9,12] (Fig. 1b). In human and mouse nasopharyngeal and intestinal lymphoid tissues, a significant proportion of mucosal B cells class-switch to $IgM^{-}IgD^{+}$B cells, which subsequentially differentiate to plasmablasts and plasma cells[1,3,5,6]. Generally, CSR to IgD (Cδ) is a less frequent event than CSR to IgG (Cγ), IgA (Cα) or IgE (Cε), perhaps a reflection among other factors of the peculiar structure of the pseudo-switch σδ region lying immediately upstream of Cδ exons. Compared to the canonical (switch) Sμ, Sγ, Sα and Sε regions lying 5' of the respective Igμ, Igγ, Igα and Igε loci, σδ is shorter and contain different nucleotide (nt) repeats[2,5,8,13,14]. These would provide an unconventional substrate for AID-mediated insertion of DSBs, possibly more prone to end resection and generation of single-strand overhangs for Sμ-σδ recombination, which leads to expression of post-recombination V_HDJ_H-*Cδ* RNA transcripts[2,8,13-15].

Unlike CSR to IgM, IgG, IgA and IgE, the mechanism of CSR to IgD remains virtually unknown. Recombination involving Sμ DSB ends with DSB ends in a downstream Sμ, Sγ, Sα and Sε region is effected by

95 non-homologous end-joining (NHEJ), one of the two major DNA DSB repair pathways, the other being
96 homologous recombination (HR)[16,17]. HR accurately repairs resected (staggered) DSB ends using a sister
97 chromatid as a homologous single-strand template during cell cycle S-G2. It critically effects error-free DSB
98 repair in somatic cells and helps orchestrate chromosome segregation in meiosis. In contrast to HR, NHEJ is a
99 homology-independent error-prone process. It synapses blunt or virtually blunt DSB ends that lack substantial
100 joining complementarity to form "direct" junctions, predominantly in G1 but also throughout the cell cycle[16].
101 NHEJ requires Ku70/Ku86 and in CSR mediates efficient long-range synapses of Sμ DSB ends with Sγ, Sα and
102 Sε DSB ends, leading to IgG, IgA and IgE[15]. The finding, however, that reduction or deletion of Ku70/Ku86
103 allowed for reduced but substantial CSR to IgG1 and IgG3 led to the postulation of an alternative CSR end-joining
104 (A-EJ) pathway[18-20]. A-EJ joins resected DSB ends, thereby giving rise to S-S junctions with microhomologies.
105 Unlike HR, however, A-EJ juxtaposes DSB ends to be joined without using a homologous template as a guide.
106 Rather, it utilizes differing extents of sequence homology between the upstream and downstream resected DSB
107 overhangs to align the to-be DNA junctions[21]. As we have shown, the HR factor Rad52 competes with Ku70/Ku86
108 for binding to S region DSB ends and synapses DSB ends by A-EJ through microhomology-mediated end-joining
109 (MMEJ)[20], as inferred from significantly increased NHEJ-mediated IgG, IgA and IgE CSR events with even fewer
110 S-S junction microhomologies in *Rad52*$^{-/-}$ B cells *in vivo* and *in vitro*[20]. This together with the increased CSR to
111 IgD in B cells lacking 53BP1, which protects S regions DSB ends from resection and facilitates long-range NHEJ
112 CSR to IgG, IgA and IgE[22-24], as well as other findings of ours showing reduced intra-Sμ DSB short-range
113 rejoining in *Rad52*$^{-/-}$ B cells[20] led us to hypothesize that by annealing to single-strand resected DSB ends, Rad52
114 mediates CSR to IgD through A-EJ involving short-range Sμ-σδ DSB recombination.

115 To test our hypothesis that Rad52 synapses Sμ with σδ DSB ends for IgD CSR, we first set up to define the
116 stimuli that consistently induce CSR to IgD in mouse and human B cells. We then used such stimuli in mouse
117 *Rad52*$^{-/-}$B cells and *RAD52* siRNA knockdown human B cells together with molecular genetic methods to
118 determine the impact of Rad52 deficiency as well as Rad52 phosphorylation on Sμ-σδ DNA recombination and
119 IgD expression. We validated our findings by analyzing specific IgD antibody and total IgD titers in mouse blood,
120 lungs and gut, as well as recombined Sμ-σδ DNA sequences in mouse spleen, mesenteric lymph nodes (MLNs)
121 and Peyer's patches as well as human tonsil B cells. We adapted chromatin immunoprecipitation (ChIP) assays
122 to analyze the recruitment of Rad52/RAD52 to the σδ region in mouse and human B cells induced to undergo
123 CSR to IgD, in which we also analyzed regulation of V_HDJ_H-*Cδ* transcription. We found that different stimuli
124 induced IgD expression by alternative splicing of long V_HDJ_H-*Cμ-s-m-Cδ-s-m* RNA transcripts or by *Sμ-σδ* CSR.
125 Further, we determined the expression of IgD by CSR to be related to Zfp318-mediated repression of the TTS
126 integrated in Cμ-Cδ loci. We correlated Sμ-σδ CSR with IgD secretion and plasma cell differentiation. Finally,
127 we analyzed B cell Rad52 phosphorylation in lupus patients and lupus-prone mice and correlated it with CSR to
128 IgD involving extensive microhomologies and somatic mutations in Sμ-σδ junctional sequences, as well as
129 occurrence of high levels of anti-nuclear antigen IgD autoantibodies. Our findings show that Rad52 mediates CSR
130 to IgD through microhomology-mediated A-EJ and in concert with Zfp318 modulation. This is a previously
131 unrecognized, critical and dedicated role of Rad52 in an essential DNA repair process in mammals.

Results

Definition of stimuli that induce Sμ-σδ CSR in mouse and human B cells. Toward testing our hypothesis that Rad52 mediates CSR to IgD, we first determined the stimuli that induce IgM^+IgD^+ B cells to undergo Sμ–σδ recombination. In these B cells, membrane IgD and secreted IgD and IgM are expressed by alternative splicing of long primary mRNA transcripts – the Cδ locus is located immediately downstream of the Cμ locus in the same transcriptional unit, allowing these two loci be coordinately regulated at the transcriptional level[1,2,4,6] (Fig. 1a). As CSR can be induced in a T-dependent or T-independent antibody fashion[15,25], we used CD40 ligand CD154 (for mouse and human B cells), TLR4 ligand LPS (mouse B cells) and TLR9 ligand CpG (human B cells) in conjunction with different cytokines and/or BCR-cross-linking to induced CSR to IgD. Recombined *Sμ–σδ, Sμ–Sγ1, Sμ–Sγ3, Sμ–Sα* and *Sμ–Sε* DNAs were detected by specific two-step nested PCRs followed by positive identification of the amplified DNA by blotting and hybridization with specific DNA probes (Fig. 1 inset) and complemented in most cases by sequencing of the junctional Sμ-σδ or Sμ-S_X DNA. Of all stimuli used, only LPS or CD154 plus IL-4 induced CSR to IgD in mouse B cells (Fig. 2a), and only CpG plus IL-2 and IL-21, or CD154 plus IL-4 or IL-15 and IL-21 induced CSR to IgD in human B cells. IgD CSR was also detected *in vivo* in tonsil B cells (Fig. 2b). The effectiveness of the stimuli that did not induce CSR to IgD was verified by the respective induction of the expected Sμ–Sγ1, Sμ–Sγ3, Sμ–Sα or Sμ–Sε DNA recombination. (IgG1, IgG3, IgA or IgE) (Fig. 2a) – no CSR to IgD, IgG, IgA or IgE occurred in *Aicda*$^{-/-}$ B cells. In all cases, CSR was further confirmed by detection of post-recombination *Iμ-Cγ1, Iμ-Cγ3, Iμ-Cα* and *Iμ-Cε* transcripts at 72 h of culture – as post-recombination Iμ-Cδ transcripts are indistinguishable from germline Iμ-Cδs-m RNA transcripts and consistent with high levels of the latter in naïve B cells, Iμ-Cδ amplification products were less abundant in class-switched IgD than naïve B cells (Figs. 1, 2c). Thus, only select stimuli induce CSR to IgD in mouse and human B cells.

Sμ-σδ junctions are enriched in microhomologies and abetted by somatic mutations in mouse and human B cells. The mechanisms effecting CSR S-S synapses can leave a S-S junctional signature[20,26]. As we previously showed, Rad52 mediates A-EJ of resected DSB ends by juxtaposing overhangs with nucleotide complementarities and, thereby, giving rise to Sμ-Sx DNA junctions with microhomologies[20]. Next generation sequencing of more than 100,000 recombined Sμ-Sx DNA junctions from mouse and human B cells *in vitro* and/or *in vivo* showed that Sμ–σδ junctions contained significantly more microhomologies (p <0.01) than Sμ–Sγ1 or Sμ–Sα DNA junctions (representative frequency and distribution of microhomologies in human and mouse B cells are depicted in Fig. 3a; representative human and mouse intra-σδ and junctional Sμ-Sx sequences are depicted in Fig. 4 and Extended Data Figs. 1,2), indicating a MMEJ[21] synaptic process underpinning Sμ–σδ junction formation. In both human and mouse B cells, the microhomologies in Sμ–σδ junctions were significantly more extensive than those in Sμ–Sγ1 and, to a lesser extent, Sμ–Sα junctions (Fig. 4, Extended Data Figs. 1,2). As one example, in human tonsil B cells, 100% of analyzed Sμ-σδ junctions contained microhomologies, consisting of 2 to 13 nucleotides (mean = 6.30), while only 21% of Sμ–Sγ1 junctions contained microhomologies, consisting of 1 to 6 nucleotides (mean = 0.72) (Fig. 3a). Interestingly, there were a few common S-S sequences shared by recombined Sμ–σδ DNA junctions in human tonsil B cells and blood naïve B cells stimulated *in vitro* by CpG plus IL-2 and IL-21, suggesting that Sμ and σδ DSB hotspots underpin Sμ–σδ in DNA recombinations. A high frequency of

169 microhomologies was also evident in the synaptic repair process of intra-σδ DSBs, evocative of what we showed
170 to be also characteristic of intra-Sμ DSBs[20]. Consistent with the greatest occurrence of microhomologies in Sμ–
171 σδ junctions, Sμ is better suited for complementary DNA single-strand annealing with σδ than Sγ1 or, to a lesser
172 extent, Sα (mouse) or Sα1 (human), based on these S regions content of various numbers and context of discrete
173 motifs, such as [G_n]AGCT repeats (Sμ, Sγ and Sα) or AGCTGAGCTG repeats (Sμ and σδ), as revealed by Pustell
174 Matrix dot-plot analysis (Fig. 3b). Finally, Sμ–σδ DNA junctions were associated with somatic point-mutations.
175 These were more frequent in the σδ area than Sμ area abetting the Sμ–σδ junction (e.g., 0.559 x 10^{-2} vs. 0.973 x
176 10^{-2} change/base in mouse spleen B cells *in vivo* and 1.251 x 10^{-2} vs. 1.985 x 10^{-2} change/base in mouse B cells
177 stimulated by LPS plus IL-4 *in vitro*) (Fig. 3c). Thus, the high frequency of microhomologies in Sμ–σδ junctions
178 supports a role of Rad52 in mediating CSR to IgD.

179 **Rad52 is critically required for Sμ–σδ recombination.** Having established that LPS or CD154 pus IL-4 induced
180 CSR to IgD in mouse B cells, we used these stimuli and *Rad52*$^{-/-}$ B cells together with appropriate controls (LPS
181 alone, LPS plus TGF-β and RA, CD154 or CD154 plus TGF-β and RA) and the same approach used in the
182 experiments of Fig. 2 to investigate whether or not Rad52 is required for CSR to IgD. Indeed, LPS plus IL-4 or
183 CD154 plus IL-4 failed to induce Sμ–σδ recombination in *Rad52*$^{-/-}$ B cells, while either treatment efficiently
184 induced Sμ-Sγ1 and Sμ-Sε DNA recombinations in the same *Rad52*$^{-/-}$ B cells, and Sμ–σδ recombination *Rad52*$^{+/+}$
185 B cells (Fig. 5a) – in *Rad52*$^{-/-}$ B cells, LPS and LPS or CD154 plus TGF-β and RA induced CSR to IgG3 and IgA,
186 respectively. As expected, CSR to IgD as well as IgG, IgA and IgE was ablated in *Aicda*$^{-/-}$ B cells. Finally, the
187 failure of *Rad52*$^{-/-}$ B cells to undergo CSR to IgD was associated with significantly decreased secretion of IgD
188 (Fig. 5b). Thus, Rad52 is critical for Sμ–σδ DNA recombination and seemingly important for IgD secretion.

189 **Rad52 is required to mount a specific IgD antibody response.** We determined the role of Rad52 in supporting
190 a specific IgD antibody response by immunizing *Rad52*$^{-/-}$ and for comparison *Rad52*$^{+/+}$ mice with OVA (20 μg
191 in alum, i.p., 3 times). *Rad52*$^{-/-}$ mice showed no Sμ–σδ recombination in spleen, mesenteric lymph nodes (MLNs)
192 or Peyer's patch B cells (Fig. 6a). The lack of CSR to IgD was specific, as B cells in such mice showed Sμ–Sγ1
193 and Sμ–Sα DNA recombinations as B cells in *Rad52*$^{+/+}$ mice, which also underwent Sμ–σδ recombination. In
194 *Rad52*$^{-/-}$ mice, Sμ–Sγ1 and Sμ–Sα DNA junctions showed fewer and shorter microhomologies than in *Rad52*$^{+/+}$
195 mice (Fig. 6b, Extended Data Figs. 2,3), a reflection of involvement of Rad52 in CSR to isotypes other than IgD[20].
196 *Rad52*$^{-/-}$ mice showed significantly decreased total and OVA-specific IgD in circulating blood, bronchoalveolar
197 lavage (BALF), feces (free or bound to fecal bacteria), and IgD-producing cells in MLNs and lamina propria, as
198 compared to their *Rad52*$^{+/+}$ counterparts (Fig. 6c-h). This contrasted with the normal or elevated total and OVA-
199 specific IgM, IgG1 and IgA levels in the same *Rad52*$^{-/-}$ mice, as predicted based on our previous findings[27]. Thus,
200 Rad52 is required to mount an efficient antigen-specific class-switched IgD response.

201 **Rad52 is modulated and phosphorylated by IgD CSR-inducing stimuli, and it is recruited to Sμ and σδ.** We
202 analyzed *Rad52, Ku70, Ku86* and *Aicda* transcripts as well as respective Rad52, Ku70, Ku86 and AID proteins,
203 including phosphorylated Rad52 (p-Rad52 has been shown to display enhanced ssDNA annealing activity[28]), in
204 B cells induced to undergo CSR to IgD. Mouse B cells stimulated by LPS plus IL-4 and human B cells stimulated

205 by CD154 plus IL-4 and IL-21 increased *Ku70/Ku86* and Ku70/Ku86 expression at 24-48 h concomitant with
206 significantly greater expression of *Aicda* and AID, which was nearly undetectable at time 0, while somewhat
207 downregulating *Rad52* and Rad52. Rad52 protein, however, was progressively phosphorylated within the same
208 time range (Fig. 7a-c). Further supporting its role in CSR to IgD, Rad52 was recruited to Sμ, σδ (and Sγ1) in B
209 cells stimulated by LPS plus IL-4, which induced Sμ-σδ (and Sμ-Sγ1) DNA recombination, but not by stimuli
210 that did not induce Sμ–σδ recombination, i.e., LPS alone or LPS plus TGF-β and RA, as shown by chromatin
211 immunoprecipitation (ChIP) using an anti-Rad52 Ab – the specificity of the ChIP Rad52 recruitment assay being
212 emphasized by the lack of chromatin immunoprecipitation in *Rad52*$^{-/-}$ B cells (Fig. 7d,e). Recruitment of Rad52
213 but not Ku70/Ku86 to σδ in CSR to IgD, as induced by LPS plus IL-4, contrasted with that of Ku70/Ku86 to Sγ3
214 and Sα regions as induced in CSR to IgG3 and IgA (Fig. 7f), a possible reflection of the competition of these HR
215 and NHEJ elements for binding to S region DSB ends[20]. Notably, LPS plus IL-4 induced recruitment of Rad52
216 but not Ku70/Ku86 to σδ, while inducing mostly Ku70/Ku86 recruitment to Cγ1, consistent with the efficient LPS
217 pus IL-4 induction of CSR to IgG1, mainly mediated by NHEJ[20]. Thus, Rad52 expression and, importantly, Rad52
218 phosphorylation are modulated by IgD CSR-inducing stimuli.

219 **Stimuli that induce Sμ-σδ DNA recombination downregulate ZFP318/Zfp318 and lead to IgD secretion.**
220 Next, we addressed the expression of mIgD and sIgD and its regulation by stimuli inducing CSR to IgD. Resting
221 B cells expressed mIgD and mIgM, but little or no sIgD or sIgM, reflecting high levels of V_HDJ_H-*Cδm* and V_HDJ_H-
222 *Cμm* trancripts and low levels of V_HDJ_H-*Cδs* and V_HDJ_H-*Cμs* transcripts (Fig. 8a). Induction of CSR to IgD (by
223 LPS or CD154 plus IL-4) resulted in loss of virtually all mIgD, emergence of V_HDJ_H-*Cδ*s transcripts together with
224 V_HDJ_H-*Cμs* transcripts and significant IgD secretion (Fig. 8a-b). By contrast, application of IgD CSR non-
225 inducing stimuli (LPS plus TGF-β and RA) to similar naive IgM$^+$IgD$^+$B cells resulted in partial loss of mIgD, no
226 change in V_HDJ_H-*Cδm* transcripts and marginal IgD secretion (Fig. 8a-b). The changes in V_HDJ_H-*Cδm,* V_HDJ_H-
227 *Cδs* transcripts, mIgD and sIgD brough about by IgD CSR-inducing stimuli paralleled the downregulation of
228 *Zfp318* transcripts and Zfp318 protein – Zfp318 represses the TTS that mediates alternative transcriptional V_HDJ_H-
229 *Cμ*/V_HDJ_H-*Cδ* termination, thereby allowing for long-range transcription throughout V_HDJ_H-*Cμ-s-m-Cδ-s-m* DNA
230 (Fig. 8c-e). Zfp318 downregulation was specific to IgD CSR, as it did not occur in response to IgA CSR-inducing
231 stimuli (LPS plus TGF-β and RA). A similar *ZFP318* downregulation concomitant with decreased mIgD
232 expression and increased IgD secretion was reproduced in human B cells submitted to IgD CSR-inducing stimuli
233 (CpG plus IL-2 and IL-21) but not IgD CSR non-inducing stimuli (CpG plus IL-4 and IL-21) (Fig. 8,f). Similarly,
234 *ZFP318* transcripts and ZFP318 protein were downregulated in human B cells undergoing IgD CSR *in vivo*, as in
235 tonsils (Fig. 8,g). It was also directly linked to very early event(s) initiating CSR to IgD, as it was independent of
236 expression of AID or Rad52, as revealed by virtual absence of *Zfp318* transcripts in LPS plus IL-4-induced *Aicda*$^-$
237 $^{/-}$ B cells, *Rad52*$^{-/-}$ B cells and *Rad52*$^{+/+}$ B cells, which all lost mIgD expression as compared to similar B cells
238 stimulated by IgA CSR-inducing stimuli (LPS plus TGF-β and RA) (Fig. 8h,i). Finally, expression of *Zfp318* in
239 B cells was not altered by *Aicda* or *Rad52* deletion (Fig. 8j). Thus, the stimuli that specifically induce CSR to
240 IgD downregulate ZFP318/Zfp318 independently of AID or Rad52 expression and prior to Sμ-σδ DNA
241 recombination.

242 **RAD52 knockdown reduces Sμ-σδ DNA recombination and IgD secretion in human B cells.** The high
243 frequency of microhomologies in Sμ-σδ junctions of human tonsil B cells *in vivo* and human B cells induced to
244 undergo CSR to IgD *in vitro* (Figs. 3a,4,6b, Extended Data Figs. 1-5) suggested to us that RAD52 also mediates
245 Sμ-σδ DNA recombination in human B cells. We purified naïve IgM^+IgD^+B cells from peripheral blood of 3
246 healthy subjects and knocked down using *RAD52*-specific siRNAs *RAD52* transcripts and RAD52 protein by up
247 to 75% and 95%, respectively. In these B cells, Sμ-σδ recombination, as induced by CpG plus IL-2 and IL-21,
248 was virtually abolished, while *AICDA* or AID expression and Sμ-Sγ1 recombination were not altered (Fig. 9a-c).
249 The reduced Sμ-σδ DNA recombination in RAD52 knockdown human B cells was associated with decreased
250 expression of V_HDJ_H-*Cδs* transcripts, without significant alteration of V_HDJ_H-*Cδm* transcripts (Fig. 9d). The
251 critical role of RAD52 in human CSR to IgD was emphasized by RAD52 recruitment to Sμ and σδ regions in
252 human naïve B cells induced to undergo CSR to IgD (by CpG plus IL-2 and IL-21) *in vitro*, human tonsil (IgD^+)
253 B cells undergoing CSR to IgD *in vivo*, but not in unstimulated naïve IgD^+IgM^+ B cells (Fig. 9e). Thus, Rad52
254 critically mediates CSR to IgD through Sμ–σδ recombination in human B cells.

255 **Sμ-σδ DNA recombination leads to IgD plasmablast/plasma cell differentiation.** To determine whether
256 induction of CSR to IgD could lead to sustained B cell IgD secretion, we analyzed plasma cell differentiation in
257 human IgM^+IgD^+B cells induced to undergo CSR to IgD by CpG plus IL-2 and IL-21. More than 13% of these
258 B cells became $mIgM^-$intracellular IgD^+ compared to about half of their counterparts stimulated by CpG plus IL-
259 4 and IL-21 and not switching to IgD (Fig. 10a). More than 90% of the IgM^-IgD^+B cells emerging from CpG
260 plus IL-2 and IL-21 simulation expressed BLIMP-1 and almost 60% were $CD27^+CD38^+$ versus about 10% of the
261 IgM^-IgD^+B cells from CpG plus IL-4 and IL-21 expressing BLIMP-1 and less than 12% being $CD27^+CD38^+$.
262 Among mouse IgM^+IgD^+B cells induced to undergo CSR to IgD by LPS plus IL-4, about 25% expressed
263 intracellular IgD. All these B cells also expressed Blimp-1 and 70% or more acquired CD138 (Fig. 10b). By
264 contrast, among IgM^+IgD^+B cells induced to undergo CSR to IgA by LPS plus TGF-β and RA, about 50%
265 expressed intracellular IgD but virtually none expressed Blimp-1 or acquired surface CD138. The relevance of
266 IgD CSR to sustained IgD secretion was further suggested by analysis of 3 human myelomas, two IgD and one
267 IgA. Both IgD myelomas showed Sμ–σδ DNA, but not Sμ–Sα DNA recombination (Fig. 10c). Conversely, the
268 IgA myeloma showed Sμ–Sα, but not Sμ–σδ DNA recombination. Thus, IgD^+ B cells emerging by CSR would
269 be prone to differentiate into IgD-secreting plasmablasts/plasma cells for sustained IgD secretion. And such IgD^+
270 B cells may function as precursors of neoplastic IgD^+ transformants.

271 **B cell Rad52 phosphorylation, increased CSR to IgD and IgD autoantibodies in systemic autoimmunity.**
272 Serum IgD have been suggested to increase in patients with inflammatory autoimmune diseases, such as systemic
273 lupus erythematosus (SLE)[29] and rheumatoid arthritis[30], and in hereditary autoinflammatory syndromes, most
274 notably the hyper-IgD syndrome (HIDS)[31-34]. In healthy humans, many B cells with CSR to IgD react with
275 components of the self[35]. We found patients with systemic lupus to display significantly higher levels of
276 circulating IgD, including IgD specific for nuclear antigens, than their healthy subject controls (Fig. 11a), possibly
277 reflecting the higher level of Rad52 and/or p-Rad52 expression. Similarly, we found lupus-prone MRL/$Fas^{lpr/lpr}$
278 mice to show far higher levels of IgD than their wildtype C57BL/6 counterparts in serum, feces and BALF as well

279 as increased IgD-coated bacteria in feces, a reflection of high levels of V_HDJ_H-$C\delta s$ transcripts in bone marrow,
280 spleen, MLNs and Peyer's patches as well as increased numbers of IgD^+ B cells in lamina propria, MLNs and
281 Peyer's patches (Fig. 11b-f). In MRL/$Fas^{lpr/lpr}$ mice, the elevated IgD levels were associated with increased IgD-
282 producing cells and increased Sμ-σδ DNA recombination in bone marrow, spleen, MLNs and Peyer's patches
283 (Fig. 11g). Increased CSR to IgD recombinations in MRL/$Fas^{lpr/lpr}$ mice were associated with high levels of p-
284 Rad52 expression, greater frequency and length of microhomologies in Sμ–σδ as compared to Sμ-Sγ1 and Sμ-
285 Sα junctional sequences, as well as with a frequency of somatic point-mutations in areas abetting Sμ-Sδ DNA
286 junctions (Fig. 11h-k and Extended Data Fig. 6). Thus, high levels of B cells expressing p-Rad52 are associated
287 with high levels of IgD and IgD autoantibodies to nuclear antigens occur in lupus patients and in lupus-prone
288 MRL/$Fas^{lpr/lpr}$ mice. In these mice, Sμ-σδ DNA recombination events involving high frequency of junctional
289 microhomologies occur in B cells of different body districts, giving rise to high levels of IgD and IgD anti-nuclear
290 antigen autoantibodies locally and systemically.

291 **Discussion**

292 The mechanism of CSR to IgG, IgA and IgE are quite well understood, as mediated by Ku70/Ku86-dependent
293 NHEJ, although occurrence of a "residual" IgM to IgG CSR in B cells lacking Ku70/Ku86 expression has
294 suggested the existence of a Ku70/Ku86-independent A-EJ synaptic mechanism[18-20]. Mice lacking 53BP1, in
295 which NHEJ-dependent CSR to IgG, IgA and IgE was significantly decreased – 52BP1 protects resection of DSB
296 ends, thereby skewing the synaptic process toward NHEJ – showed increased CSR to IgD and increased
297 circulating IgD levels, suggesting that the short-range Sμ–σδ CSR was mediated by a 53BP1-independent synaptic
298 process involving resected DSB ends[22,23]. This together with our previous demonstration that Rad52 plays a
299 central role in the MMEJ process that synapses intra-Sμ region resected DSB ends as well as *c-Myc/IgH* locus
300 translocations also involving resected DSB ends[20] prompted us to hypothesize that Rad52 is central to the A-EJ
301 process that synapses Sμ and σδ DSB resected ends with complementary overhangs in CSR to IgD. Here, we
302 demonstrated that Rad52 mediates CSR to IgD in mouse and human B cells (Extended Data Fig. 7), thereby
303 unveiling a previously unknown, critical and dedicated role of this HR factor in mammalian DNA repair.

304 We have provided unequivocal evidence that Rad52 is critical for CSR to IgD *in vitro* and *in vivo,* in mouse
305 and human B cells. In mouse *Rad52*$^{-/-}$ B cells, Sμ-σδ DNA recombination was ablated and IgD secretion greatly
306 reduced. Similarly, in *RAD52* knockdown B cells from healthy subjects, Sμ-σδ DNA recombination was virtually
307 abrogated and IgD secretion greatly decreased – as expected[1,5], Sμ-σδ DNA recombination could not occur in the
308 absence of AID, which introduces DSBs in σδ as it does in Sμ, Sγ, Sα or Sε. In mouse *Rad52*$^{-/-}$ B cells and
309 human *RAD52* knockdown B cells, decreased post-recombination V_HDJ_H-*Cδs* transcripts resulted in reduced IgD
310 secretion and occurred in the presence of unaltered transmembrane V_HDJ_H-*Cδm* transcript levels, at least within
311 the first 72 hours from CSR induction. Interestingly, the stimuli that selectively induced CSR to IgD modulated
312 the overall levels of *Ku70/KU70*, *Ku86/KU86* and *Rad52/RAD52* transcripts while significantly upregulating
313 *Aicda/AICDA* in mouse and human B cells. This was concomitant with induction of AID and moderate decrease
314 in Rad52 protein, which, in fact, was increasingly phosphorylated at Tyr104. Rad52 phosphorylation at Tyr104
315 has been shown to boost Rad52-mediated DNA single-strand annealing and is possibly effected by c-ABL
316 kinase[28]. Rad52 involvement in CSR to IgD was further emphasized by recruitment of this protein to σδ region
317 (in addition to, necessarily, Sμ) *in vivo*, in mouse spleen B cells and human tonsil IgD$^+$ B cells, as well as *in vitro*,
318 in mouse and human naïve B cells induced to undergo CSR to IgD, but not in similar B cells undergoing CSR to
319 IgG3 or IgA. Instead, these B cells recruited Ku70/Ku86 to Sγ3 and Sα, consistent with the major contribution
320 of NHEJ to CSR to IgG3 and IgA.

321 Rad52 is a member of the eponymous epistasis group for DSB repair that shows strong evolutionary
322 conservation[17,36]. In *Saccharomyces cerevisiae,* Rad52 is a key element of the HR pathway, and its deletion or
323 mutation impairs DNA DSB repair[37,38]. Indeed, yeast Rad52 is a recombination mediator and a facilitator of
324 annealing of complementary DNA single-strands[39,40]. It functions as a cofactor of Rad51, which forms
325 nucleoprotein filaments with single-strand DNA and promotes strand pairing, by overcoming the inhibitory effect
326 of replication protein A (RPA)[41]. By contrast, Rad52 mutation or even deletion results in no obvious abnormalities
327 in viability or functions in mammalian cells. As we have shown, *Rad52*$^{-/-}$ mice displayed no significant alteration

328 of immune system elements, including B cells, or functions[20], possibly owing to the presence of mammalian gene
329 paralogues, such as *BRCA2* and *RAD51*, which by encoding functions related to Rad52, can compensate for the
330 absence of this factor[42]. Human BRCA2 functions as a recombination mediator by facilitating RAD51
331 nucleoprotein filament formation[40,43-45]. Nevertheless, human BRCA2 cannot facilitate annealing of RPA-coated
332 DNA, a function that Rad52 carries out efficiently in the absence of BRCA2[46]. This together with Rad52
333 involvement in DSB repair at stalled or collapsed replication forks points at a unique role of Rad52 in catalyzing
334 single-strand annealing in homology-directed DNA repair in human cells[47-49].

335 Our identification of Rad52 as essential in Sμ-σδ synapses that underpins CSR to IgD provides, to the best of
336 our knowledge, the first demonstration of a critical and dedicated role of this factor n mammalian DNA repair.
337 The short-range Rad52-mediated Sμ-σδ recombination of resected DSB ends adds to the other Rad52-mediated
338 short-range DSB recombination we recently uncovered: intra-Sμ region DSB recombination[20]. This, like Sμ–σδ
339 synapsing, engages resected DSB ends and yields significant junctional nucleotide microhomologies[20]. In this
340 function, as in CSR to IgD, Rad52 is not fungible in mouse or human B cells. Our identification of Rad52 as the
341 critical element in Sμ-σδ synapsis also sheds light on the mechanistic nature of the CSR A-EJ DSB repair pathway
342 (originally referred to as A-NHEJ[19]). As per our current findings, such the CSR A-EJ pathway uses the HR Rad52
343 to synapse upstream and downstream DSB overhangs by a MMEJ process but does not require a homologous
344 template as a guide as the HR pathway does. DNA polymerase θ has been suggested to contribute to A-EJ[21]. Our
345 previous findings, however, did not support a role of this polymerase in Rad52-mediated intra-Sμ DSB
346 recombination or Sμ–Sγ1, Sμ–Sγ3, Sμ–Sγ2a/Sγ2c and Sμ–Sα recombination (CSR to IgG1, IgG3, IgG2a/IgG2c
347 and IgA)[20]. Finally, while (MMEJ) A-EJ functions as a back-up pathway in cells defective in NHEJ or HR, it also
348 synapses DSB ends in cells that are competent for both NHEJ and HR[50], as exemplified by the microhomologies
349 in S-S junctions in B cells that class switched to IgG, IgA and IgE and the disappearance of such microhomologies
350 upon Rad52 ablation[20].

351 As we showed here, Rad52 works in concert with Zfp318 to modulate IgD expression through an interplay of
352 alternative RNA splicing and DNA recombination, the latter after AID intervention. Zfp318 represses the TTS
353 intercalated between the Cμ and Cδ exons within the *Ighμ/Ighδ* loci transcriptional complex unit[10,11], thereby
354 allowing for transcription of long primary V_HDJ_H-*Cμ-s-m-Cδ-s-m* RNA. Zfp318, however, would also
355 simultaneously allow for the continuous expression of primary *Iμ-Cμ-s-m-Cδ-s-m* RNA transcripts. In fact, albeit
356 possibly more abundant, hence their predominant detection in our specific PCR assays, *Iμ-Cδ* transcripts – in
357 secretory or membrane form – are identical in sequence to their post-recombination *Iμ-Cδ* counterparts (Fig. 1a,b).
358 During developmental transition from mature to immature B cells, Zfp318 expression closely parallels mIgD
359 expression[10,11]. Consistent with its repression of the TTS intercalated between the *Cμ* and *Cδ* exons complex, the
360 Zfp318 protein is expressed during the transition from immature IgM^+IgD^- to mature IgM^+IgD^{hi} B cell[10,11]. And,
361 as we showed here, naïve mature B cells which express high levels of mIgD also express high levels of *Zfp318*
362 transcripts and Zfp318 protein. In these B cells, stimuli that induced Sμ-σδ DNA recombination, yielding primary
363 V_HDJ_H-*Cδ-s-m* RNA transcripts, also induced profound downregulation of *Zfp318* transcripts and Zfp318 protein,
364 suggesting that relieving Zfp318-mediated TTS repression is a prerequisite for Sμ-σδ DNA recombination to

365 unfold. Conversely, as we also showed here, naïve mature IgM^+IgD^+ B cells submitted to stimuli that induced
366 CSR to isotypes other than IgD, such as IgA (by LPS plus IL-4 and RA), further upregulated *Zfp318* transcripts
367 and Zfp318 protein, concomitant with no Sμ-σδ DNA recombination, thereby allowing for massive expression of
368 mIgD rather than sIgD.

369 The role of Zfp318 as gene transcription regulator is highly specific for IgD, as genome-wide transcriptome
370 analysis of B cell Zfp318-deficient mice identified *Sva* as the only other gene altered in expression[11] –
371 interestingly, *Sva* is also involved in alternative splicing, albeit outside the *IgH* locus[51]. Zfp318 would be under
372 the control of 5'AMP-activated protein kinase (Ampk). This is phosphorylated by Lbk1[52], whose signaling
373 triggers the B cell GC reaction. Indeed, Lbk1's failure to activate Ampk or Ampk loss specifically muted Zfp318
374 expression and IgD transcription[52]. In contrast, activation of Ampk by phenformin impaired GC formation[52],
375 likely by heightening Zfp318 expression, possibly in addition to other mechanisms. This would result in increased
376 expression of primary V_HDJ_H-*Cμ-s-m-Cδ-s-m* RNA transcripts but not Sμ-σδ DNA recombination, suggesting
377 that CSR to IgD is one of the multiple and complex events inherent to GC formation. This is triggered by naturally
378 occurring generally microbial stimuli, as in tonsil GCs and GCs or other secondary lymphoid formations in
379 aerodigestive mucosae[1,5,6]. Consistent with the contention that Ampk mediates the regulation of Zfp318 as well
380 as the contrasting impact of IgD CSR-inducing (LPS plus IL-4) and non-inducing stimuli (LPS plus TGF-β and
381 RA) on expression of Zfp318, stimulation of both human and mouse cells by LPS has been shown to result in
382 dephosphorylation/inactivation of Ampk, while similar cell stimulation by TGF-β resulted in rapid
383 phosphorylation/activation of this protein kinase[53].

384 In our experiments, stimuli that induced CSR to IgD (e.g., LPS plus IL-4 in mouse B cells, and CD154 plus
385 IL-2 and IL-21 in human B cells) also downregulated Zfp318 expression which, in turn, reduced V_HDJ_H-*Cδm*
386 transcript level and mIgD, while greatly increasing V_HDJ_H-*Cδs* transcripts and secreted IgD. This argues for CSR
387 to IgD to be critical for significant IgD secretion. Interestingly, stimuli that induced Sμ-σδ recombination and
388 IgD secretion also induced plasmablast/plasma cell differentiation, as shown by Blimp-1 and $C38^+CD27^+$
389 expression in human B cells, and Blimp-1 and $CD138^+$ in mouse B cells. A similar outcome was not produced
390 by stimuli that did not induce Sμ-σδ recombination and IgD secretion in mouse or human B cells. Thus, while
391 alternative splicing of long primary V_HDJ_H-*Cμ-s-m-Cδ-s-m* RNA transcripts in B cells that have not undergo CSR
392 would make some contribution to the overall level of IgD production *in vivo*, CSR to IgD is likely required for
393 substantial and sustained IgD production, as secreted by plasmablasts/plasma cells or by neoplastic transformants,
394 such as IgD myeloma cells. The limited IgD amounts detected in supernatants of mouse or human B cells primed
395 by stimuli that induced high levels of mIgD but not Sμ–σδ synaptic recombination would result from translation
396 of alternative spliced long primary V_HDJ_H-*Cμ-s-m-Cδ-s-m* RNA transcripts as well as some "shedding" of mIgD.

397 Bacteria and viruses have been suggested to play an important role in driving CSR to IgD, generally through
398 stimulation of TLRs in gut and respiratory lymphoid tissues, and mesenteric lymph nodes, possibly leading to
399 emergence of plasmablasts and plasma cells secreting IgD[1,3-5,51,54-56]. Circulating IgD are increased in patients
400 with frequent respiratory infections or chronic lung inflammation suggesting a protective role for this Ig

401 isotype[1,3,5,56]. Our findings support the notion that both T-dependent (CD154) and T-independent (TLR ligands)
402 stimuli induce Sμ-σδ DNA recombination, in combination with various cytokines[1,4-6]. Interestingly, although we
403 previously showed that BCR-signaling synergizes with TLR-signaling for induction of AID and CSR to IgG and
404 IgA[25], BCR signaling did not synergize with TLR7 or TLR9 signaling to induce CSR to IgD, as shown by the lack
405 of Sμ-σδ DNA recombination in B cells stimulated by CpG or R848 plus IL-4 and anti-Igδ Ab. In the *in vivo* T-
406 dependent antibody response to OVA, ablation of CSR to IgD (*Rad52*$^{-/-}$ mice) resulted in reduced levels of total
407 and specific IgD in circulating blood and BALF, decreased total and/or bacteria-bound IgD in feces as well as
408 decreased numbers of IgD^{+} B cells lamina propria and MLNs, a privileged site of IgD CSR[12]. As predicted by
409 our previous findings[20], the overall decreased IgD levels in *Rad52*$^{-/-}$ mice were associated with increased IgG1
410 and IgA as well as greatly decreased frequency and lengths of microhomologies in Sμ-Sγ1 and Sμ-Sα junctions.
411 This reflected the lack of Rad52 contribution to the synaptic process underpinning such junctions as well as the
412 lack of Rad52 competition with Ku70/Ku86[20], which resulted solely in Ku70/Ku86-mediated NHEJ, a process
413 that limits microhomologies to 0-3 nt[16].

414 Information on the contribution of IgD to autoimmunity is scant and contradictory. IgD that bind self-antigens
415 and are mostly polyreactive occur in healthy subjects, much like IgM or even IgG and IgA do[35,57-60]. High levels
416 of IgD have been reported in rheumatoid arthritis patients and thought to possibly be implicated in the
417 pathogenesis of the disease[30]. mIgD expression, however, has been speculated to exert an inhibitory effect on B
418 cell autoreactivity, as suggested by elevated autoantibody production, increased deposition of immune complexes
419 in kidneys and severe nephritis in lupus-prone C56BL/6*lpr* mice with deletion of the Igδ locus[61,62]. Our findings
420 unequivocally showed that total and self-reactive IgD (dsDNA, histone, RNP/Sm or RNA and ANAs) to be
421 elevated in the circulation of lupus patients and lupus-prone MRL/*Fas*$^{lpr/lpr}$ mice. The latter displayed higher
422 levels of total IgD in serum, BALF and feces, than their wildtype C57BL/6 counterparts. Such high IgD levels
423 reflected Sμ-σδ DNA recombinations which included Sμ-σδ junctions with extensive microhomologies and high
424 frequency of somatic mutations in the DNA areas abetting Sμ-σδ junctions. IgD class-switched B cells occurred
425 at high numbers in different districts, such as bone marrow, spleen, MLNs and Peyer's patches. This together
426 with the B cell high levels of p-Rad52 and the low levels Zfp318 indicated that in murine and likely human lupus,
427 IgD autoantibodies stem from extensive B cell Sμ-σδ recombination rather than alternative splicing of primary
428 V_HDJ_H-*Cμ-s-m-Cδ-s-m* RNA transcripts. Thus, our findings do not suggest a "protective" role of IgD in
429 autoimmunity[61,62], while rather supporting a role of IgD in systemic lupus autoantibody responses.

430 Collectively, our findings outline a critical and dedicated role of Rad52 in mediating the synapsis of Sμ with
431 σδ DSB resected ends. They also provide the first demonstration of Rad52 as a critical element in the poorly
432 understood contribution of A-EJ to the resolution of DSBs in nonmalignant cells. In malignant B cells, Rad52 is
433 involved in DNA recombination events that give rise to DNA deletions and translocations. As we previously
434 showed, Rad52 ablation reduced the frequency of *c-Myc/IgH* translocations in mouse *p53*$^{-/-}$ B cells by more than
435 70%, with the residual translocations containing limited microhomologies[20]. Whether Rad52 intervention extends
436 to other modalities of A-EJ in neoplastic and non-neoplastic lymphoid mammalian cells remains to be determined.
437 The importance of this newly unveiled and essential function of Rad52 is further emphasized by our demonstration

438 that this highly conserved HR element is critical for CSR to IgD in both mouse and human B cells. This together
439 with the further reduction of the physiologically moderate microhomologies in Sμ–Sγ1, Sμ–Sγ3, Sμ–Sα and Sμ–
440 Sε junctions in *Rad52*$^{-/-}$ B cells (current data and refs.[18-20]) solidifies the role of Rad52 as critical mediator of the
441 A-EJ backup pathway underpinning the residual CSR to IgG, IgA and IgE in the absence of Ku70/Ku86 proteins[20].
442 Our findings also showed how stimuli that induce Sμ-σδ recombination coordinate Rad52 function, as enabled
443 by phosphorylation, with downregulation of Zfp318, unique repressor of the TTS intercalated between the Cμ and
444 Cδ loci, whose activity allows transcription throughout V_HDJ_H-*Sμ-Cμ-s-m-σδ-Cδ-s-m* and *Iμ-Cμ-s-m-σδ-Cδ-s-m*.
445 Further, they indicate that CSR to IgD is required for sustained IgD secretion and possibly a prerequisite for IgD
446 plasmablast/plasma cell differentiation. They also add new and significant information to a potential role of CSR
447 to IgD, as promoted by Rad52 phosphorylation, in systemic autoimmunity. Finally, they provide important
448 molecular information to approach the virtually unexplored mechanistic underpinning of hyper-IgD syndrome, a
449 relatively rare but a severe autoinflammatory disease associated with mevalonate kinase deficiency (due to *MVK*
450 recessive mutations) and exorbitant levels of IgD[31,32,63].

451

452 **Acknowledgements**

453 We thank Dr. Patrick M. Sung for reviewing this manuscript. We also would like to thank Amanda Fisher, Dr.
454 Justin B. Moroney, Dr. Helia N. Sanchez and Dr. Huoqun Gan for their help in some experiments. This work was
455 supported by NIH grants R01 AI 079705, T32 AI138944, R01 AI 105813 and the Lupus Research Alliance Target
456 Identification in Lupus Grant 641363 to P.C.

457 **Methods**

458 **Mice.** *Rad52*$^{-/-}$ mice were generated by replacing exon 3 of the *Rad52* gene with positive selection marker
459 neomycin, as driven by the phosphoglycerate kinase (PGK) promoter, and an upstream mouse sequence
460 functioning as a transcription terminator (Dr. Albert Pastink, Leiden University, Leiden, The Netherlands)[36].
461 *Rad52*$^{-/-}$ mice were backcrossed to C57/BL6 mice for more than six generations. No full length or truncated
462 Rad52 protein was produced from the disrupted allele[36]. *Rad52*$^{-/-}$ mice were viable and fertile, and showed no
463 gross abnormalities. *Aicda*$^{-/-}$ mice (C57BL/6 background)[64] were obtained from Dr. Tasuku Honjo (Kyoto
464 University, Kyoto, Japan). C57BL/6 and MRL/*Fas*$^{lpr/lpr}$ mice were purchased from Jackson Laboratory (Bar
465 Harbor, Maine). All mice were housed in pathogen-free conditions. Both male and female mice aged 8-12 weeks
466 were used for the experiments. The Institutional Animal Care and Use Committees (IACUC) of the University
467 of Texas Health Science Center at San Antonio approved all animal protocols.

468 **Mouse B cells and CSR induction *in vitro*.** Naïve IgM$^+$IgD$^+$B cells were isolated from spleens of 8–12-week-
469 old C57BL/6, *Rad52*$^{-/-}$ or *Aicda*$^{-/-}$ mice as described[25]. B cells were resuspended in RPMI 1640 medium with
470 10% FBS (FBS-RPMI), 50 mM β-mercaptoethanol and 1x antibiotic-antimycotic mixture (15240-062; Invitrogen)
471 and stimulated with LPS (4 μg/ml) from *Escherichia coli* (055:B5; Sigma-Aldrich), CD154 (1 U/ml; obtained
472 from membrane fragments of baculovirus-infected Sf21 insect cells[25]), CpG ODN 1826 (1.0 μM; Eurofins
473 Genomics) or R848 (1.0 μM; Medkoo) plus nil, IL-4 (5.0 ng/ml; R&D Systems) and/or TGF-β (2.0 ng/ml; R&D
474 Systems) and retinoic acid (RA, 10 nM) or anti-BCR Ab (anti-δ mAb-dextran, 30 ng/ml; Fina Biosolutions).
475 Mouse B cells were cultured in FBS-RPMI at 37°C in 48-well plates for 24, 48, 72 and 96 h.

476 **Human B cells and CSR induction *in vitro*.** Naïve IgM$^+$IgD$^+$B cells were purified by negative selection using
477 the EasySep™ human naive B cell enrichment kit (19254; StemCell Technologies) from healthy subject PBMCs,
478 following manufacturer's instructions. Tonsillar IgD$^+$ B cells were isolated from human tonsil cells by positive
479 selection using biotin-anti-human IgD mAb (clone IA6-2; 348212, Biolegend) and MagniSort™ Streptavidin
480 Positive Selection Beads (MSPB-6003-74, Thermo Fisher Scientific). Naïve B cells were stimulated with CD154
481 (10 U/ml) or CpG ODN 2395 (1.0 μM; Eurofins Genomics) plus nil, IL-2 (20 ng/ml; BioLegend), IL-4 (20 ng/ml;
482 R&D Systems), IL-15 and/or IL-21 (50 ng/ml; R&D Systems). Human B cells were cultured in FBS-RPMI at
483 37°C in 48-well plates for 24, 48, 72, 96 and 120 h.

484 **Flow cytometry.** For surface staining, mononuclear cells were reacted with VF-anti-CD19 mAb (75-0193-0100,
485 Tonbo), PE-anti-IgM mAb (clone RMM1, 406507, BioLegend), and FITC anti-mouse IgD mAb (clone 11-26c.2a,
486 405704, BioLegend) and 7-AAD. For intracellular staining, cells were stained with anti-CD19 mAb (Clone 1D3;
487 Tonbo) and fixable viability dye eFluor® 450 (FVD 450, eBiosciences) followed by incubation with the BD
488 Cytofix/Cytoperm buffer at 4°C for 20 min. After washing twice with the BD Perm/Wash buffer, cells were
489 resuspended in HBSS with 1% BSA and stored overnight at 4°C. Cells were then stained with anti-Zfp318 Ab
490 (AAS23325C, Antibody Verify; labeled with FITC using iLink™ Antibody Labeling Kits, ABP Biosciences).
491 FACS analysis was performed on single cell suspensions. In all flow cytometry experiments, cells were
492 appropriately gated on forward and side scattering to exclude dead cells and debris. Cell analyses were performed

493 using a LSR-II flow cytometer (BD Biosciences), and data were analyzed using FlowJo software (TreeStar). All
494 experiments were performed in triplicates.

495 **Fluorescence microscopy.** Fluorescence microscopy of tissues. To analyze IgM and IgD-producing cells in the
496 lamina propria and PPs, the intestine was folded into a "Swiss-roll", fixed with PFA (4%), and embedded in
497 paraffin. Ten μm sections were cut and heated at 80 °C to adhere to the slide, washed four times in xylene for
498 2 min, dehydrated two times with 100% ethanol for 1 min, two times with 95% ethanol for 1 min and washed two
499 times in water for 1 min. Antigens were unmasked using 2 mM EDTA in 100 °C for 40 mins followed by a cooling
500 step at 25 °C on the bench top, 3 times washing with 1x TBS and blocking using 10% BSA for 15 min. Slides
501 were again washed 3 times with 1x TBS and stained with FITC–anti-IgD mAb (clone 11-26c.2a; 405713,
502 BioLegend), PE goat-anti-mouse-IgM mAb (406507, BioLegend) for 2 h in a dark moist chamber. After washing
503 3 times with Triton X-100 (0.1%) in TBS, slides were air dried, and cover slips were mounted with ProLong®
504 Gold Antifade Reagent with DAPI (Invitrogen). Fluorescence images were captured using a 10x objective lens
505 with a Zeiss Axio Imager Z1 fluorescence microscope. To analyze IgD-producing cells in MLNs, 10 μm MLN
506 sections were prepared by cryostat and loaded onto positively charged slides, fixed in cold acetone and stained
507 with FITC–anti-IgD mAb (405704, BioLegend), or PE goat-anti-mouse-IgM mAb (406507, BioLegend),
508 respectively, for 1 h at 25 °C in a moist chamber. Cover slips were then mounted using ProLong® Gold Antifade
509 Reagent using DAPI (Thermo Fisher), before examination with a fluorescence microscope.

510 Fluorescence microscopy of B cells. B cells were suspended at 10^5 cells/100 μl in FCS-RPMI. Pre-labeled
511 slides were then placed into Cytofunnels and ran with 50 μl of FCS-RPMI in order to wet the Cytofunnel paper.
512 Cells were then placed again into the Cytofunnel and spun at 800 RPM for 3 min using a Cytospin™ 4
513 Cytocentrifuge (Thermo Fisher). For intracellular visualization of IgM, IgD, CD138 and Blimp-1 proteins, cells
514 were fixed with methanol for 15 min and washed 3 times in PBS-Tween 20. Cells were then blocked in 10% BSA
515 for 15 min and stained with 1:20 APC-anti-mouse IgD Ab (clone 11-26c.2a; 405713, BioLegend), FITC-anti-
516 mouse IgM mAb (11-5790-81, Thermo Fisher), overnight in a dark moist chamber.

517 **Detection of free and bacterial-bound antibodies.** Titers of serum, BALF or fecal total IgD, IgM, IgG1 and IgA
518 and OVA-binding IgD, IgM, IgG1 and IgA were measured using specific ELISAs, as we described[20,25,65,66]. Total
519 IgD in *in vitro* culture supernatants of stimulated human and mouse B cells or in serum, BALF or feces were
520 measured by dot blotting with serially two-fold diluted samples.

521 Bacteria-bound IgD and IgA were detected in feces by flow cytometry, as we described[27]. Feces (10 mg)
522 were suspended in 100 μl 1x PBS (filtered through 0.2 μm filter), homogenized and centrifuged at 400 × g for 5
523 min to remove large particles. The supernatant was then centrifuged at 8000 g for 10 min to remove non-bound
524 antibodies (in supernatant). The bacterial pellet was suspended in 1 ml of PBS with 1% (w/v) BSA. After fixation
525 with 7.2% formaldehyde for 10 min at room temperature, bacteria were washed with PBS, and stained with FITC–
526 anti-IgD mAb (clone 11-26c.2a; 405713, BioLegend) or FITC-anti-IgA mAb (C10-3, BD Biosciences) on ice for
527 30 min, washed with PBS, and further resuspended in 1 x PBS containing 0.2 μg ml^{-1} DAPI for flow cytometry
528 analysis. All events that stained with DAPI were considered as bacteria.

529 **S-S region DNA recombinations and S region somatic mutations.** Genomic DNA was prepared from human
530 or mouse B cells using QIAmp DNA Mini Kit (Qiagen), or from paraffin-embedded human IgD or IgA myeloma
531 tissue sections (obtained from the University of Arkansas for Medical Science) using Quick-DNA™ FFPE Kit
532 (Zymo Research). Recombined Sμ–σδ, Sμ–Sγ1, Sμ–Sα and Sμ–Sε DNA were amplified by two sequential rounds
533 of specific PCR using Phusion™ high-fidelity DNA polymerase (Thermo Scientific™) and nested oligonucleotide
534 primers[67] (**Supplementary Table 1**). The first and second rounds of PCR were performed at 98 °C for 30 sec,
535 58 °C for 45 sec, 72 °C for 4 min (30 cycles). Amplified DNA was fractionated through 1.0% agarose, blotted
536 onto Hybond-N^+ membranes (GE Healthcare) and hybridized to biotin-labeled Sμ and σδ, Sγ1, Sα or Sε specific
537 probes. Detection was performed using the Chemiluminescent Nucleic Acid Detection Module (Thermo Fisher
538 Scientific) according to the manufacturer's instructions. For sequence analysis of the recombined DNA, PCR
539 products were purified using a QIAquick PCR purification kit (Qiagen). The amplified library was tagged with
540 barcodes for sample multiplexing, and PCR was enriched and annealed to the required Illumina clustering adapters.
541 High-throughput 300–base pair (bp) paired-end sequencing was performed by the UTHSCSA Genome
542 Sequencing Facility using the Illumina MiSeq platform. S-S junctions and somatic mutations in the S regions
543 were analyzed by sequence alignment as performed by comparing PCR products sequences with germline Sμ and
544 σδ, Sγ1 or Sα sequences using National Center for Biotechnology Information BLAST
545 (www.ncbi.nih.gov/BLAST).

546 **RT-PCR and quantitative RT-PCR (qRT-PCR).** For quantification of mRNA, germline I_H-C_H, post-
547 recombination Iμ-C_H and mature V_HDJ_H-C_H transcripts, RNA was extracted from 0.2-5.0 x 10^6 cells using either
548 Trizol® Reagent (Invitrogen) or RNeasy Plus Mini Kit (Qiagen). Residual DNA was removed from the extracted
549 RNA with gDNA eliminator columns (Qiagen). cDNA was synthesized from total RNA with the SuperScript™
550 IV First-Strand Synthesis System (Thermo Fisher) using oligo-dT primer. Transcript expression was measured
551 by qRT-PCR with the appropriate primers (Supplemental Table 1) using a Bio-Rad MyiQ™ Real-Time PCR
552 Detection System (Bio-Rad Laboratories) to measure SYBR Green (IQ™ SYBR® Green Supermix, Bio-Rad
553 Laboratories) incorporation with the following protocol: 95°C for 15 sec, 40 cycles of 94°C for 10 sec, 60°C for
554 30 sec, 72°C for 30 sec. Data acquisition was performed during 72°C extension step. Melting curve analysis was
555 performed from 72°C-95°C. Mature V_HDJ_H-$C\mu m$, V_HDJ_H-$C\mu s$, V_HDJ_H-$C\delta m$ and V_HDJ_H-$C\delta s$ transcripts were
556 analyzed by semi-quantitative PCR using serially two-fold diluted cDNA.

557 **Western blotting.** B cells were lysed in Laemmli buffer. Cell extracts containing equal amounts of protein (50-
558 100 μg) were fractionated through SDS-PAGE (6%). The fractionated proteins were transferred onto
559 polyvinylidene difluoride membranes (Bio-Rad) overnight (30 V/90 mA) at 4 °C. After blocking and overnight
560 incubation at 4 °C with anti-AID antibody (H-80, Santa Cruz), anti-Ku70 antibody (A0883, Abclonal), anti-Ku86
561 antibody (A5862, Abclonal), anti-Rad52 antibody (H-300, Santa Cruz Biotechnology), anti-phospho-Rad52
562 antibody (Y408472, Applied Biological Materials Inc.) or anti-β-Actin mAb (2F1-1, BioLegend), the membranes
563 were incubated with horseradish peroxidase (HRP)-conjugated secondary antibodies. After washing with TBS–
564 Tween 20 (0.05%), bound HRP-conjugated antibodies were detected using Western Lightning Plus-ECL reagents

565 (PerkinElmer Life and Analytical Sciences).

566 **ChIP and qPCR.** ChIP assays were performed as previously described[68-70]. Human or mouse B cells (1.0 x 10^7)
567 were treated with formaldehyde (1% v/v) for 10 min at 25°C to crosslink chromatin, washed once in cold PBS
568 with protease inhibitors (Roche) and resuspended in lysis buffer (20 mM Tris-HCl, 200 mM NaCl, 2 mM EDTA,
569 0.1% w/v SDS and protease inhibitors, pH 8.0). Chromatin was fragmented by sonication (DNA fragments of
570 about 200 to 1,000 bp in length), pre-cleared with protein A agarose beads (Pierce) and incubated with agarose
571 conjugated anti-Rad52 mAb (clone F-7; sc-365341 AC, Santa Cruz Biotechnology) at 4°C overnight. Immune
572 complexes were washed and eluted (50 mM Tris-HCl, 0.5% SDS, 200 mM NaCl, 100 μg/ml proteinase K, pH
573 8.0), followed by incubation at 65°C for 4 h. DNA was purified using a QIAquick PCR purification kit (Qiagen).
574 The Sμ or σδ region DNA was amplified from immunoprecipitated chromatin by qPCR using appropriate primers
575 (**Supplemental Table 1**). Data were normalized to input chromatin DNA and depicted as relative abundance of
576 each amplicon.

577 ***RAD52* knockdown in human B cells.** The human RAD52-specific siRNA oligo duplex (TT320001, Locus ID
578 5893) and non-effective Trilencer-27 Flurescent-labeled transfection control siRNA duplex (SR30002) were
579 obtained from Origene Technologies. The siRNA duplexes were used to transfect purified human naïve B cells
580 using the Human B Cell Nucleofector™ Kit (VPA-1001, LONZA). Transfected B cells were then stimulated with
581 CpG ODN 2395 plus IL-2 and IL-21 for 96 h before genomic DNA extraction for analysis of Sμ-σδ and Sμ-Sγ1
582 DNA recombination. Expression of *RAD52* and *AICDA* transcripts were analyzed by qRT-PCR using specific
583 primers 24 h after transfection. Expression of RAD52, phosphorylated-RAD52, AID and β-ACTIN proteins were
584 analyzed by immune-blotting 24 h after transfection.

585 **High-throughput mRNA-Seq.** RNA was isolated from cells using the Directzol RNA Microprep Kit (Zymogen
586 Research), according to manufacturer's instructions and as previously described[66]. RNA integrity was verified
587 using an Agilent Bioanalyzer 2100 (Agilent). Next generation RNA-Seq for mRNA and non-coding RNA was
588 performed by the Genome Sequencing Facility at University of Texas Health Science Center San Antonio Greehey
589 Children's Cancer Research Institute. High-quality RNA was processed using an Illumina TruSeq RNA sample
590 prep kit v2 or TruSeq Small RNA Sample Prep kit following the manufacturer's instructions (Illumina). Clusters
591 were generated using TruSeq Single-Read Cluster Gen. Kit v3-cBot-HS on an Illumina cBot Cluster Generation
592 Station. After quality control procedures, individual mRNA-Seq or small RNA-Seq libraries were then pooled
593 based on their respective 6-bp index portion of the TruSeq adapters and sequenced at 50 bp/sequence using an
594 Illumina HiSeq 3000 sequencer. Resulting reads were checked by assurance (QA) pipeline and initial genome
595 alignment (Alignment). After the sequencing run, demultiplexing with CASAVA was employed to generate the
596 Fastq file for each sample. All sequencing reads were aligned with their reference genome (UCSC mouse genome
597 build mm9) using TopHat2 default settings, and the Bam files from alignment were processed using HTSeq-count
598 to obtain the counts per gene in all samples. Quality control statistical analysis of outliers, intergroup variability
599 and distribution levels, were performed for statistical validation of the experimental data.

600 **Statistical analysis.** Statistical analysis was performed using Excel (Microsoft) or Prism® GraphPad software.

601 *P*-values were determined by paired and unpaired Student's *t*-tests; and *P*-values <0.05 were considered
602 significant.

603 **IRB for use of human tissues and peripheral blood as well as IACUC for use of mice**. For the use of DNA
604 procured from formalin fixed paraffin embedded tissues obtained from the University of Arkansas for Medical
605 Science, the study was reviewed by the University of Arkansas for Medical Sciences Institutional Review Board
606 (IRB) which determined that this project is not human subject research as defined in 45 CFR 46.102. Human B
607 cells were purified from PBMCs of healthy subject buffy coats obtained from South Texas Blood and Tissue
608 Center, San Antonio, Texas, under the *Healthy Volunteer Blood Donor Program* and lupus patients B cells were
609 purified PBMCs obtained under the Long School of Medicine IRB HSC 20140234H *Class switching, somatic*
610 *hypermutation and plasma cell differentiation in B cells.* Mouse and mouse B cell studies were performed under
611 the Long School of Medicine IACUC 20200019AR *Somatic hypermutation, class switch DNA recombination and*
612 *plasma cell differentiation in antibody and autoantibody responses.*

613 **Figure legends**

614 **Fig. 1 | Expression of cell surface and secreted IgD and IgM, as well as Iμ-Cδ transcripts by alternative**
615 **splicing, alternative transcription termination and CSR. a**, Schematics of alternative splicing and alternative
616 transcription termination for expression of membrane and secreted IgM and IgD, as well as germline *Iμ-Cμ* and
617 *Iμ-Cδ* transcripts in B cells. In the presence of Zfp318, which represses the transcription termination sites (TTS)
618 of the Cμ gene, mature B cells constitutively transcribe long primary V_HDJ_H-*Cμ-Cδs–m* transcripts initiated by the
619 V_H promoter. These long primary transcripts undergo alternative splicing which removes intronic regions, leading
620 to dual expression of mature V_HDJ_H-*Cμs* and V_HDJ_H-*Cδm* transcripts encoding IgM and IgD. In the absence of
621 Zfp318, transcription stops at Cμ TTS, resulting in a shorter primary transcript, which does not contain Cδ exons,
622 and lead to expression of a mature V_HDJ_H-*Cμ–s–m* transcript only. Mature B cells also transcribe *Iμ, Cμ,* and *Cδ*
623 regions under control of the Iμ promoter. When Zfp318 is present, unswitched mature B cells constitutively
624 transcribe long primary *Iμ-Cμ–s–m-Cδ–s–m* transcripts, which undergo alternative splicing to removes intronic
625 regions, leading to dual expression of germline *Iμ-Cμ* and *Iμ-Cδ* transcripts. In the absence of Zfp318, *Iμ*
626 promoter-initiated transcription stops at Cμ TTS, and only germline Iμ-Cμ transcripts are expressed. **b,** Expression
627 of membrane and secreted IgD, and *Iμ-Cδ* transcripts by CSR. Schematic representation of CSR from IgM to
628 IgD. The Sμ region recombines with the σδ region and loops out the intervening DNA, which forms a switch circle.
629 The recombined DNA is transcribed leading to expression of V_HDJ_H-*Cδ–s–m* and *Iμ-Cδ* transcripts, initiated by
630 the V_H and Iμ promoters, respectively. In this case, *Iμ-Cδ* transcripts are generated as post-recombination
631 transcripts. Graphics depict portion of the *IgH* locus and the resulting primary and mature transcripts. The inset
632 depicts a schematic representation of the detection of Sμ–σδ junctional DNA (CSR to IgD) by nested PCR
633 amplification followed by Southern-blotting using specific Sμ and σδ probes (Southern-blotting of amplified
634 recombined Sμ–σδ DNA from human naïve and germinal center B cells). In many cases the amplified Sμ-σδ DNA
635 was sequenced for further analysis of junctional sequence well as dentification and census of mutations. iEμ, *IgH*
636 intronic enhancer; Iμ, intervening μ exon; μm, exon encoding the transmembrane region of IgM; δm, exon
637 encoding the secretory piece of IgM; σδ, noncanonical switch-like region 5′ to Cδ; δs, exon encoding the secretory
638 region of IgD; Cδm, exon encoding the transmembrane region of IgD. Dotted gray lines show splicing
639 configurations of primary transcripts to yield secreted and transmembrane forms of IgM and IgD.

640 **Fig. 2 | Identification of stimuli inducing CSR to IgD and Sμ-σδ junctions in mouse and human B cells. a,**
641 Wildtype C57BL/6 and *Aicda*$^{-/-}$ mouse naïve B cells were stimulated with nil, LPS, LPS plus IL-4, LPS plus TGF-
642 β and RA, CD154, CD154 plus IL-4, CD154 plus TGF-β and RA, CpG, CpG plus IL-4, CpG plus TGF-β and RA,
643 R848, R848 plus IL-4, R848 plus TGF-β and RA, or CpG plus IL-4, or R848 plus IL-4 in the presence of anti-BCR.
644 Recombined Sμ-σδ, as well as Sμ-Sγ1, Sμ-Sγ3, Sμ-Sα and Sμ-Sα DNA were analyzed 72 or 96 h post-stimulation
645 by nested long-range PCR using forward Iμ and reverse Cδ primers, or forward Iμ and reverse Sγ1, Sγ3, Sα or Sε
646 primers, respectively, followed by Southern-blotting using a specific Sμ, σδ, Sγ1, Sγ3, Sα or Sε probe, as indicated.
647 **b,** Recombined Sμ-σδ DNA in human tonsil IgD$^+$ B cells, blood naive B cells, or blood naive B cells stimulated with
648 CD145 or CpG plus IL-2 and IL-21, IL-4 and IL-21, or IL-2, IL-4 and IL-21 or IL-15 and Il-21, were analyzed 96 or
649 120 h post-stimulation by nested long-range PCR using forward Iμ and reverse Cδ primers, followed by Southern-

650 blotting using specific human Sμ or σδ probe. Data are one representative of 3 independent experiments yielding
651 comparable results. **c,** Germline/post-recombination Iμ-Cδ transcripts, post-recombination Iμ-Cγ1, Iμ-Cα and Iμ-
652 Cε transcripts in wildtype C57BL/6 B cells stimulated with nil, LPS plus IL-4, or LPS plus TGF-β and RA, analyzed
653 72 h post-stimulation by qRT-PCR and normalized to *β-Actin* expression. Each dot represents data obtained with
654 B cells from an individual mouse ($n = 3$ per group). Data are mean ± SEM.

655 **Fig. 3 | Mouse and human Sμ-σδ DNA recombination junctions contain microhomologies and somatic**
656 **mutations. a,** Amplified junctional DNAs of intra-σδ deletions, as well as Sμ-σδ, Sμ-Sγ1 and Sμ-Sα1
657 recombination from OVA-immunized C57BL/6 mouse spleen B cells, C57BL/6 mouse naïve B cells stimulated
658 with LPS plus IL-4 and cultured for 96 h, as well as human tonsil B cells or human peripheral blood naïve B cells
659 stimulated with CpG plus IL-2 and IL-21 and cultured for 96 or 120 h were sequenced by MiSeq. The length and
660 numbers of nucleotide overlaps (microhomologies) in intra-σδ deletions, Sμ-σδ, Sμ-Sγ1 and Sμ-Sα1 junctional
661 DNAs are shown by violin plots. Each dot represents a unique junctional sequence ($n = 45$ per group). **b,** Mouse
662 and human Sμ and σδ regions consist of repetitive motifs, which are better suited substrates for Rad52-mediated
663 MMEJ than those in Sμ and Sγ1 or Sμ and Sα. As such, they can facilitate the formation of microhomologies.
664 Repetitive sequence elements in mouse and human Sμ, σδ, Sγ1 and Sα that can potentially form microhomologies
665 were identified by Pustell Matrix dot plot using MacVector software and are depicted by small dots. Intensity of
666 dots depicts frequency and degree of complementarity of respective sequences. **c**, Somatic point-mutations in Sμ
667 and σδ regions abetting recombined Sμ–σδ DNA junctions in IgD class-switched mouse and human B cells *in vitro*
668 and *in vivo.* Mutations were identified in a 48 to 506 nt stretch of Sμ or σδ regions in unique Sμ-σδ DNA
669 recombination sequences. Each dot represents an individual sequence. Sequence data were pooled from 3
670 individuals in each group. In pie charts, the size of slices denotes the proportion of sequences with the same
671 number of mutations and the grey hue denotes the number of point-mutations per sequence; below the pie charts
672 is the overall mutation frequency (change/base). $^{**}p < 0.01$, $^{***}p < 0.001$, ns: not significant (unpaired *t* test).

673 **Fig. 4 | *In vivo* human Sμ-σδ DNA recombination junctions contain high frequencies of microhomologies.**
674 Amplified intra-σδ deletional, Sμ-σδ, Sμ-Sγ1 and Sμ-Sα1 junctional DNAs from human tonsil B cells were
675 sequenced using MiSeq system. Thirty-two intra-σδ, Sμ-σδ, Sμ-Sγ1 or Sμ-Sα1 junction sequences are shown in
676 each column. Each sequence is compared with the corresponding germline Sμ (above, blue) and σδ, Sγ1 or Sα1
677 (below, red) sequences. Microhomologies (bold) were determined by identifying the longest region at the Sμ-σδ,
678 Sμ-Sγ1 or Sμ-Sα1 junction of perfect uninterrupted donor/acceptor identity or the longest overlap region at the
679 S–S junction with no more than one mismatch on either side of the breakpoint.

680 **Fig. 5 | Rad52 mediates Sμ-σδ DNA recombination leading to IgD secretion. a,** Recombined Sμ-σδ, Sμ-Sγ1,
681 Sμ-Sα and Sμ-Sε DNA in mouse *Rad52*$^{+/+}$, *Rad52*$^{-/-}$ and *Aicda*$^{-/-}$ naïve B cells stimulated with nil, LPS only, LPS
682 plus IL-4, LPS plus TGF-β and RA, CD154 only, CD154 plus IL-4, or CD154 plus TGF-β and RA, as well as Sμ-
683 Sγ3 in *Rad52*$^{+/+}$, *Rad52*$^{-/-}$ and *Aicda*$^{-/-}$B cells stimulated with LPS only, were analyzed 96 h post stimulation by
684 nested long-range PCR using forward Iμ and reverse Cδ, Sγ1, Sγ3, Sα or Sε primers, respectively, followed by
685 Southern-blotting using specific Sμ, σδ, Sγ1, Sγ3, Sα or Sε probe, as indicated. Data are one representative of 3

686 independent experiments yielding comparable results. **b,** IgD titers in culture (96 h) fluid of *Rad52*$^{+/+}$ and *Rad52*$^{-}$
687 $^{/-}$B cells stimulated with LPS plus IL-4, as measured by dot-blotting (two-fold serial diluted culture fluid) using a
688 rat anti-mouse IgD mAb. Data are one representative of 5 independent experiments yielding comparable results.

689 **Fig. 6 | *Rad52* deletion ablates *in vivo* Sμ-σδ DNA recombination and reduces IgD production.** *Rad52*$^{+/+}$ and
690 *Rad52*$^{-/-}$ mice were immunized (i.p.) with OVA. **a,** Recombined Sμ-σδ, Sμ-Sγ1, and Sμ-Sα DNA in spleen,
691 mesenteric lymph nodes (MLN) and Peyer's patches B cells, as analyzed by nested long-range PCR using forward
692 Iμ and reverse Cδ, Sγ1 or Sα primers, followed by Southern-blotting using specific Sμ, σδ, Sγ1 or Sα probe, as
693 indicated. Data are one representative of 3 independent experiments yielding comparable results. **b,** Sμ-σδ, Sμ-
694 Sγ1 and Sμ-Sα junctional DNAs were amplified by nested PCR and sequenced using by MiSeq. The length and
695 numbers of nucleotide overlaps (microhomologies) in Sμ-σδ, Sμ-Sγ1 and Sμ-Sα junctional DNAs are shown by
696 violin plots. Each symbol represents a unique sequence (n = 45 per group). **c-f,** Titers of total IgD in serum,
697 BALF and feces, as analyzed by dot-blotting using rat anti-mouse IgD mAb. Titers of total IgM, IgD, IgG1 and IgA
698 as well as OVA-binding IgM, IgD, IgG1 and IgA as analyzed by specific ELISAs. Each dot represents data from
699 one individual mouse (n = 5-8 per group, pooled from two experiments). *$p < 0.05$, **$p < 0.01$, ***$p < 0.001$, ns: not
700 significant (unpaired t test). **g,** Bacteria-bound IgD and IgA in feces as analyzed by flow cytometry. **h,** IgM, IgD
701 and IgA positive cells in mesenteric lymph nodes (MLNs) and lamina propria as visualized by fluorescence
702 microscopy. Data in **g,h** are representative of 3 independent experiments.

703 **Fig. 7 | Rad52 is phosphorylated and recruited to Sμ and σδ in B cells induced to undergo IgD CSR. a,**
704 C57BL/6 mouse naïve B cells were stimulated with LPS plus IL-4 and cultured for 0, 24, 48, 72 and 96 h. *Rad52*,
705 *Ku70*, *Ku86* and *Aicda* transcripts were analyzed by real-time qRT–PCR, normalized to *β-Actin* expression and
706 depicted as relative to the expression in unstimulated B cells (set as 1.0). Data are mean ± SEM of 3 independent
707 experiments. **b,** Expression of Rad52, phosphorylated Rad52 (p-Rad52), AID, Ku70, Ku86, and β-Actin proteins
708 in mouse B cells stimulated with LPS plus IL-4 (as in **a**), as analyzed by specific immunoblotting. Data are one
709 representative of 3 independent experiments yielding comparable results. **c,** Human peripheral blood naive B cells
710 were stimulated with CD154 plus IL-4 and IL-21 and cultured for 0, 24, 48, 72 and 96 h. *RAD52*, *KU70*, *KU86* and
711 *AICDA* transcripts were analyzed by real-time qRT-PCR, normalized to *β-ACTIN* expression and depicted as
712 relative to the expression in unstimulated B cells (set as 1.0). Data are mean ± SEM of 3 independent experiments.
713 **d,** Recruitment of Rad52 to σδ region DNA, as analyzed by ChIP-qPCR assays in mouse *Rad52*$^{+/+}$ and *Rad52*$^{-/}$B
714 cells stimulated with LPS plus IL-4 and cultured for 72 h. Data are expressed as percent of pre-IP input for each
715 sample (mean ± SEM). **e,f,** C57BL/6 mouse B cells were stimulated with nil, LPS, LPS plus IL-4 or LPS plus TGF-
716 β and RA and cultured for 72 h. Recruitment of Rad52 (**e**) and Ku70/Ku86 (**f**) to Sμ, σδ, Sγ1, Sγ3 and Sα region
717 DNA, as analyzed by ChIP-qPCR assays. Data are mean ± SEM of 3 independent experiments.

718 **Fig. 8 | Stimuli inducing Sμ-σδ DNA recombination downregulate ZFP318/Zfp318 in human and mouse B**
719 **cells. a**, C57BL/6 mouse naïve B cells were stimulated with nil, LPS plus IL-4 or LPS plus TGF-β and RA. Surface
720 expression of IgM and IgD were analyzed 96 h post stimulation by flow cytometry. Expression of V_HDJ_H-$C\delta$–m,
721 V_HDJ_H-$C\delta$–s, V_HDJ_H-$C\mu$–m and V_HDJ_H-$C\mu$–s transcripts were analyzed 72 h post-stimulation by semi-quantitative

722 RT-PCR using serial two-fold dilution of cDNA templates. Data are representative of 3 independent experiments.
723 **b,** IgD in supernatant from cultures (96 h) of C57BL/6 mouse naïve B cell stimulated with nil, LPS plus IL-4, LPS
724 plus TGF-β and RA, or CD154 plus IL-4, as analyzed by dot-blotting using rat anti-mouse IgD mAb. Data are
725 representative of 5 independent experiments. **c,** Expression of *Zfp318* transcripts in mouse naïve B cells
726 stimulated with nil, LPS plus IL-4, or LPS plus TGF-β and RA, as analyzed 72 h post-stimulation by qRT-PCR and
727 normalized to *β-Actin* expression and depicted relative to the average expression in unstimulated B cells (set as
728 1). Data are mean ± SEM of 3 independent experiments. **d,** Expression of *Zfp318* transcripts in mouse naïve B
729 cells stimulated with LPS plus IL-4, as analyzed 96 h post-stimulation by mRNA-Seq. Data are mean ± SEM of 4
730 independent experiments. **e,** Zfp318 protein level in mouse naïve B cells stimulated with nil, LPS plus IL-4, or LPS
731 plus TGF-β and RA, as analyzed 96 h post-stimulation by intracellular staining with rabbit anti-Zfp318 Ab in flow
732 cytometry. Bars on the right panel represent the MFI (mean ± SEM) from 3 independent experiments. **f,** Human
733 blood naïve B cells stimulated with nil, CpG plus IL-2 and IL-21 or CpG plus IL-4 and IL-21. Human V_HDJ_H-*Cδ–m*,
734 V_HDJ_H-*Cδ–s*, V_HDJ_H-*Cμ–m* and V_HDJ_H-*Cμ–s* transcript levels were measured 72 h post-stimulation by semi-
735 quantitative RT-PCR with serial two-fold dilution of cDNA templates – data are representative of 3 independent
736 experiments (left panels). Expression of *ZFP318* transcripts as analyzed 72 h post-stimulation by qRT-PCR and
737 normalized to *HPRT* expression (**f** middle panel) – data are mean ± SEM of 3 independent experiments. Secreted
738 IgD in supernatants of the human B cell cultures, as analyzed 120 h post stimulation by specific ELISA (**f** right
739 panel) – data are mean ± SEM of 4 independent experiments. **g,** Expression of V_HDJ_H-*Cδ–m*, V_HDJ_H-*Cδ–s*, V_HDJ_H-
740 *Cμ–m* and V_HDJ_H-*Cμ–s* transcripts in human total IgD^+ tonsil B cells, as analyzed by semi-quantitative RT-PCR
741 involving serial two-fold dilution of cDNA templates (left panel) – data are representative of 3 independent
742 experiments. Expression of ZFP318 protein in human tonsil IgM^+IgD^+B cells and IgM^-IgD^+B cells, as analyzed by
743 intracellular staining with anti-Zfp318 Ab in flow cytometry (middle panel) – data are representative of 4
744 independent experiments (mean ± SEM, right panel). **h,** Surface expression of IgM and IgD in mouse naïve
745 *Rad52*$^{+/+}$, *Rad52*$^{-/-}$ and *Aicda*$^{-/-}$B cells stimulated with LPS plus IL-4, or LPS plus TGF-β and RA, as analyzed 96
746 h post-stimulation by flow cytometry. Data are representative of 3 independent experiments. **i,** Expression of
747 V_HDJ_H-*Cδ–m* and V_HDJ_H-*Cδ–s* transcripts in mouse naïve *Rad52*$^{+/+}$ and *Rad52*$^{-/-}$B cells stimulated with nil, LPS
748 plus IL-4 or LPS plus TGF-β and RA, as analyzed 72 h post-stimulation by semi-quantitative RT-PCR using serial
749 two-fold dilution of cDNA templates. Data are representative of 3 independent experiments. **j,** Rad52 or AID
750 deficiency does not alter *Zfp318* expression. Expression of *Zfp318* transcripts in mouse naïve *Rad52*$^{+/+}$, *Rad52*$^{-}$
751 $^{/-}$ and *Aicda*$^{-/-}$B cells stimulated with nil, LPS plus IL-4, or LPS plus TGF-β and RA, as analyzed 72 h post-
752 stimulation by qRT-PCR and normalized to *β-Actin* expression, as depicted relative to expression in unstimulated
753 B cells (set as 1). Data are mean ± SEM of 3 independent experiments.

754 **Fig. 9 | RAD52 is required for Sμ-σδ DNA recombination in human B cells. a,** Human blood naïve IgM^+IgD^+B
755 cells were transfected with specific *RAD52* siRNA or scrambled (Scra) siRNA and stimulated by CpG plus IL-2
756 and IL-21. Recombined Sμ-σδ and Sμ-Sγ1 DNA in the transfected B cells 120 h after siRNA transfection, as well
757 as Sμ-σδ DNA in tonsil IgM^-IgD^+ and blood naive IgM^+IgD^+B cells were analyzed by nested long-range PCR using
758 forward Iμ and reverse Cδ or Sγ1 primers followed by Southern-blotting using indicated specific probes. Data are

759 from 3 independent experiments. **b**, Expression of *RAD52* and *AICDA* transcripts was analyzed 48 h after siRNA
760 transfection by qRT-PCR and normalized to *HPRT* expression. Data are mean ± SEM of 3 independent
761 experiments. **c**, Expression of RAD52 and AID proteins were analyzed 72 h after siRNA transfection by specific
762 immunoblotting. Data are representative of 3 independent experiments. **d**, Expression of V_HDJ_H-*Cδm* and V_HDJ_H-
763 *Cδs* transcripts as analyzed by semi-quantitative RT-PCR with of serial two-fold dilution of cDNA templates. Data
764 are representative of 3 independent experiments. **e,** RAD52 is recruited to σδ region DNA in human B cells
765 undergoing CSR to IgD. Recruitment of RAD52 to Sμ and σδ region DNA in human blood B cells stimulated for
766 120 h with CpG plus IL-2 and IL-21, as analyzed by specific ChIP-qPCR. Data are mean ± SEM of 3 or 4
767 independent experiments.

768 **Fig. 10 | B cells undergoing CSR to IgD differentiate to IgD-producing plasmablasts/plasma cells. a,** Human
769 B cells stimulated with CpG plus IL-2 and IL-21, which induce IgD CSR, or CpG plus IL-4 and IL-21, which do not
770 induce IgD CSR. Proportions of $CD138^+IgD^+IgM^-$ plasmablasts/plasma cells among intracellular $sIgM^-IgD^+$B cells
771 and Blimp1 expression in intracellular IgD^+sIgM^- cells, as analyzed 120 h post stimulation by flow cytometry. **b,**
772 mouse *Rad52*$^{+/+}$ and *Rad52*$^{-/-}$B cells stimulated with LPS plus IL-4, which induce IgD CSR. Proportions of
773 $sCD138^+$ plasmablasts/plasma cells among intracellular IgD^+sIgM^- cells and Blimp1 expression in intracellular
774 IgD^+sIgM^- cells, as analyzed 96 h post stimulation by flow cytometry. Data in **a** and **b** are representative of 3
775 independent experiments. **c,** Recombined Sμ-σδ and Sμ-Sα DNA in two IgD^+ myelomas and one IgA^+ myeloma
776 as analyzed by nested long-range PCR followed by Southern-blotting using indicated probes.

777 **Fig. 11 | p-Rad52 expression, CSR to IgD and anti-nuclear antigen IgD autoantibodies in lupus mice and**
778 **patients. a,** Concentrations of total, and dsDNA-, RNA-, histone- or RNP/Sm-binding IgD in healthy human
779 subjects and SLE patients, as analyzed by specific ELISAs. Data are mean ± SEM of 6 to 10 healthy subjects or
780 SLE patients. **b,** Concentrations of total IgD in serum, feces and BALF as analyzed by dot-blotting, and
781 concentrations of dsDNA- or histone-binding IgD autoantibodies in serum of C57BL/6 and MRL/*Fas*$^{lpr/lpr}$ mice as
782 analyzed by specific ELISAs. Data are mean ± SEM of 3 to 9 mice. **c,** IgD concentrations in the serum, BALF and
783 feces of C57BL/6 and MRL/*Fas*$^{lpr/lpr}$ mice, as analyzed by dot-blotting. Shown are dot-blots from one C57BL/6
784 and one MRL/*Fas*$^{lpr/lpr}$ mouse, representative of 3 to 9 C57BL/6 and MRL/*Fas*$^{lpr/lpr}$ mice. Expression of V_HDJ_H-
785 *Cδm,* V_HDJ_H-*Cδs,* V_HDJ_H-*Cμm* and V_HDJ_H-*Cμs* transcripts in bone marrow (BM), spleen and mesenteric lymph
786 nodes (MLNs) as analyzed semi-quantitative RT-PCR in serial two-fold dilutions of cDNA templates. Shown are
787 RT-PCR data from one C57BL/6 and one MRL/*Fas*$^{lpr/lpr}$ mouse, representative of 3 C57BL/6 and 3 MRL/*Fas*$^{lpr/lpr}$
788 mice. **d,** ANAs as visualized by indirect immunofluorescence on HEp-2 cells that were incubated with sera from
789 a human healthy subject and a SLE patient or C57BL/6 and MRL/*Fas*$^{lp/lpr}$ mice and revealed using FITC-labeled
790 rat mAb to mouse IgD. **e,** Bacteria-bound IgD and IgA in feces of C57BL/6 and MRL/*Fas*$^{lpr/lpr}$ mice, as analyzed
791 by flow cytometry. **f,** IgD^+B cells in lamina propria, MLNs and Peyer's patches of C57BL/6 and MRL/*Fas*$^{lpr/lpr}$ mice,
792 as visualized by fluorescent microscopy. **g,** Recombined Sμ-σδ, Sμ-Sγ1, and Sμ-Sα DNA in bone marrow, spleen,
793 MLNs and Peyer's patches B cells from C57BL/6 and MRL/*Fas*$^{lpr/lpr}$ mice were analyzed by nested long-range
794 PCR using forward Iμ and reverse Cδ, Sγ1 or Sα primers, followed by Southern-blotting using indicated probes.
795 Data are representative of 3 independent experiments. **h,** Sμ-σδ, Sμ-Sγ1 and Sμ-Sα junctional DNAs in non-

796 immunized MRL/*Fas*$^{lpr/lpr}$ mice, as amplified by nested PCR and sequenced by MiSeq. The length and numbers
797 of nucleotide overlaps (microhomologies) in Sμ-σδ, Sμ-Sγ1 and Sμ-Sα junctional DNAs are shown by violin plots.
798 Each dot represents a unique sequence (n = 45 per group). **i**, Somatic point-mutations in Sμ and σδ regions
799 abetting recombined Sμ–σδ DNA junctions in IgD class-switched spleen B cells from 3 MRL/*Fas*$^{lpr/lpr}$ mice.
800 Mutations were identified in a 48 to 506 nt stretch of Sμ or σδ regions in unique Sμ-σδ DNA recombination
801 sequences. Each dot represents an individual sequence. In pie charts, the size of slices denotes the proportion
802 of sequences with the same number of mutations and the grey hue denotes the number of point-mutations per
803 sequence; below the pie charts is the overall mutation frequency (change/base). $^{**}p < 0.05$, $^{**}p < 0.01$,
804 $^{***}p < 0.001$, ns: not significant (unpaired t test). **j,** Expression of *Zfp318* and *Aicda* transcripts in MLNs from non-
805 immunized C57BL/6 and MRL/*Fas*$^{lpr/lpr}$ mice as analyzed by specific qRT-PCR. Data are mean ± SEM of 3
806 C57BL/6 and 3 MRL/*Fas*$^{lpr/lpr}$ mice. **k,** Expression of phosphorylated Rad52 (p-Rad52), Rad52 and β-Actin
807 proteins in peripheral blood B cells from healthy human subjects and SLE patients as well as B cells from non-
808 immunized C57BL/6 and MRL/*Fas*$^{lpr/lpr}$ mice, as analyzed by specific Western blotting using rabbit anti-p-Rad52
809 Ab (Y408472, Applied Biological Materials Inc.) or anti-β-Actin mAb (2F1-1, BioLegend). P-Rd52 (Y104) Ab
810 detected endogenous levels of Rad52 protein only when phosphorylated at tyrosine 104.

811 **References**

812 1. Chen, K., Xu, W., Wilson, M., He, B., Miller, N.W., Bengten, E., Edholm, E.S., Santini, P.A., Rath, P., Chiu, A.,
813 Cattalini, M., Litzman, J., J, B.B., Huang, B., Meini, A., Riesbeck, K., Cunningham-Rundles, C., Plebani, A. & Cerutti,
814 A. Immunoglobulin D enhances immune surveillance by activating antimicrobial, proinflammatory and B cell-
815 stimulating programs in basophils. *Nat Immunol* **10**, 889-898 (2009).

816 2. Chen, K. & Cerutti, A. New insights into the enigma of immunoglobulin D. *Immunol Rev* **237**, 160-179 (2010).

817 3. Cerutti, A., Chen, K. & Chorny, A. Immunoglobulin responses at the mucosal interface. *Annu Rev Immunol* **29**, 273-293
818 (2011).

819 4. Chen, K. & Cerutti, A. The function and regulation of immunoglobulin D. *Curr Opin Immunol* **23**, 345-352 (2011).

820 5. Choi, J.H., Wang, K.W., Zhang, D., Zhan, X., Wang, T., Bu, C.H., Behrendt, C.L., Zeng, M., Wang, Y., Misawa, T., Li,
821 X., Tang, M., Zhan, X., Scott, L., Hildebrand, S., Murray, A.R., Moresco, E.M., Hooper, L.V. & Beutler, B. IgD class
822 switching is initiated by microbiota and limited to mucosa-associated lymphoid tissue in mice. *Proc Natl Acad Sci U S*
823 *A* **114**, E1196-E1204 (2017).

824 6. Chen, K., Magri, G., Grasset, E.K. & Cerutti, A. Rethinking mucosal antibody responses: IgM, IgG and IgD join IgA.
825 *Nat Rev Immunol* **20**, 427–441 (2020).

826 7. Ohta, Y. & Flajnik, M. IgD, like IgM, is a primordial immunoglobulin class perpetuated in most jawed vertebrates. *Proc*
827 *Natl Acad Sci U S A* **103**, 10723-10728 (2006).

828 8. Gutzeit, C., Chen, K. & Cerutti, A. The enigmatic function of IgD: some answers at last. *Eur J Immunol* **48**, 1101-1113
829 (2018).

830 9. Shan, M., Carrillo, J., Yeste, A., Gutzeit, C., Segura-Garzon, D., Walland, A.C., Pybus, M., Grasset, E.K., Yeiser, J.R.,
831 Matthews, D.B., van de Veen, W., Comerma, L., He, B., Boonpiyathad, T., Lee, H., Blanco, J., Osborne, L.C., Siracusa,
832 M.C., Akdis, M., Artis, D., Mehandru, S., Sampson, H.A., Berin, M.C., Chen, K. & Cerutti, A. Secreted IgD Amplifies
833 Humoral T Helper 2 Cell Responses by Binding Basophils via Galectin-9 and CD44. *Immunity* **49**, 709-724 (2018).

834 10. Enders, A., Short, A., Miosge, L.A., Bergmann, H., Sontani, Y., Bertram, E.M., Whittle, B., Balakishnan, B., Yoshida,
835 K., Sjollema, G., Field, M.A., Andrews, T.D., Hagiwara, H. & Goodnow, C.C. Zinc-finger protein ZFP318 is essential
836 for expression of IgD, the alternatively spliced Igh product made by mature B lymphocytes. *Proc Natl Acad Sci U S A*
837 **111**, 4513-4518 (2014).

838 11. Pioli, P.D., Debnath, I., Weis, J.J. & Weis, J.H. Zfp318 regulates IgD expression by abrogating transcription termination
839 within the Ighm/Ighd locus. *J Immunol* **193**, 2546-2553 (2014).

840 12. Rouaud, P., Saintamand, A., Saad, F., Carrion, C., Lecardeur, S., Cogne, M. & Denizot, Y. Elucidation of the enigmatic
841 IgD class-switch recombination via germline deletion of the IgH 3' regulatory region. *J Exp Med* **211**, 975-985 (2014).

842 13. Kluin, P.M., Kayano, H., Zani, V.J., Kluin-Nelemans, H.C., Tucker, P.W., Satterwhite, E. & Dyer, M.J. IgD class
843 switching: identification of a novel recombination site in neoplastic and normal B cells. *Eur J Immunol* **25**, 3504-3508
844 (1995).

845 14. Arpin, C., de Bouteiller, O., Razanajaona, D., Fugier-Vivier, I., Briere, F., Banchereau, J., Lebecque, S. & Liu, Y.J. The
846 normal counterpart of IgD myeloma cells in germinal center displays extensively mutated IgVH gene, Cm-Cd switch,
847 and lambda light chain expression. *J Exp Med* **187**, 1169-1178 (1998).

848 15. Xu, Z., Zan, H., Pone, E.J., Mai, T. & Casali, P. Immunoglobulin class-switch DNA recombination: induction, targeting
849 and beyond. *Nat Rev Immunol* **12**, 517-531 (2012).

850 16. Pannunzio, N.R., Watanabe, G. & Lieber, M.R. Nonhomologous DNA end-joining for repair of DNA double-strand
851 breaks. *J Biol Chem* **293**, 10512-10523 (2018).

852 17. Wright, W.D., Shah, S.S. & Heyer, W.D. Homologous recombination and the repair of DNA double-strand breaks. *J*
853 *Biol Chem* **293**, 10524-10535 (2018).

854 18. Yan, C.T., Boboila, C., Souza, E.K., Franco, S., Hickernell, T.R., Murphy, M., Gumaste, S., Geyer, M., Zarrin, A.A.,
855 Manis, J.P., Rajewsky, K. & Alt, F.W. IgH class switching and translocations use a robust non-classical end-joining
856 pathway. *Nature* **449**, 478-482 (2007).

857 19. Boboila, C., Yan, C., Wesemann, D.R., Jankovic, M., Wang, J.H., Manis, J., Nussenzweig, A., Nussenzweig, M. & Alt,
858 F.W. Alternative end-joining catalyzes class switch recombination in the absence of both Ku70 and DNA ligase 4. *J Exp*
859 *Med* **207**, 417-427 (2010).

860 20. Zan, H., Tat, C., Qiu, Z., Taylor, J.R., Guerrero, J.A., Shen, T. & Casali, P. Rad52 competes with Ku70/Ku86 for binding
861 to S-region DSB ends to modulate antibody class-switch DNA recombination. *Nat Commun* **8**, 14244 (2017).

862 21. Sallmyr, A. & Tomkinson, A.E. Repair of DNA double-strand breaks by mammalian alternative end-joining pathways.
863 *J Biol Chem* **293**, 10536-10546 (2018).

22. Bothmer, A., Robbiani, D.F., Feldhahn, N., Gazumyan, A., Nussenzweig, A. & Nussenzweig, M.C. 53BP1 regulates DNA resection and the choice between classical and alternative end joining during class switch recombination. *J Exp Med* **207**, 855-865 (2010).
23. Bothmer, A., Robbiani, D.F., Di Virgilio, M., Bunting, S.F., Klein, I.A., Feldhahn, N., Barlow, J., Chen, H.T., Bosque, D., Callen, E., Nussenzweig, A. & Nussenzweig, M.C. Regulation of DNA end joining, resection, and immunoglobulin class switch recombination by 53BP1. *Mol Cell* **42**, 319-329 (2011).
24. Marini, F., Rawal, C.C., Liberi, G. & Pellicioli, A. Regulation of DNA Double Strand Breaks Processing: Focus on Barriers. *Front Mol Biosci* **6**, 55 (2019).
25. Pone, E.J., Zhang, J., Mai, T., White, C.A., Li, G., Sakakura, J.K., Patel, P.J., Al-Qahtani, A., Zan, H., Xu, Z. & Casali, P. BCR-signalling synergizes with TLR-signalling for induction of AID and immunoglobulin class-switching through the non-canonical NF-kappaB pathway. *Nat Commun* **3**, 767 (2012).
26. Wu, X., Tsai, C.Y., Patam, M.B., Zan, H., Chen, J.P., Lipkin, S.M. & Casali, P. A role for the MutL mismatch repair Mlh3 protein in immunoglobulin class switch DNA recombination and somatic hypermutation. *J Immunol* **176**, 5426-5437 (2006).
27. Sanchez, H.N., Moroney, J.B., Gan, H., Shen, T., Im, J.L., Li, T., Taylor, J.R., Zan, H. & Casali, P. B cell-intrinsic epigenetic modulation of antibody responses by dietary fiber-derived short-chain fatty acids. *Nat Commun* **11**, 60 (2020).
28. Honda, M., Okuno, Y., Yoo, J., Ha, T. & Spies, M. Tyrosine phosphorylation enhances RAD52-mediated annealing by modulating its DNA binding. *EMBO J* **30**, 3368-3382 (2011).
29. Kantor, G.L., Van Herle, A.J. & Barnett, E.V. Auto-antibodies of the IgD class. *Clin Exp Immunol* **6**, 951-962 (1970).
30. Wu, Y., Chen, W., Chen, H., Zhang, L., Chang, Y., Yan, S., Dai, X., Ma, Y., Huang, Q. & Wei, W. The elevated secreted immunoglobulin D enhanced the activation of peripheral blood mononuclear cells in rheumatoid arthritis. *PLoS One* **11**, e0147788 (2016).
31. Drenth, J.P., Cuisset, L., Grateau, G., Vasseur, C., van de Velde-Visser, S.D., de Jong, J.G., Beckmann, J.S., van der Meer, J.W. & Delpech, M. Mutations in the gene encoding mevalonate kinase cause hyper-IgD and periodic fever syndrome. International Hyper-IgD Study Group. *Nat Genet* **22**, 178-181 (1999).
32. Hager, E.J., Tse, H.M., Piganelli, J.D., Gupta, M., Baetscher, M., Tse, T.E., Pappu, A.S., Steiner, R.D., Hoffmann, G.F. & Gibson, K.M. Deletion of a single mevalonate kinase (Mvk) allele yields a murine model of hyper-IgD syndrome. *J Inherit Metab Dis* **30**, 888-895 (2007).
33. Ammouri, W., Cuisset, L., Rouaghe, S., Rolland, M.O., Delpech, M., Grateau, G. & Ravet, N. Diagnostic value of serum immunoglobulinaemia D level in patients with a clinical suspicion of hyper IgD syndrome. *Rheumatology (Oxford)* **46**, 1597-1600 (2007).
34. Govindaraj, G.M., Jain, A., Peethambaran, G., Bhoyar, R.C., Vellarikkal, S.K., Ganapati, A., Sandhya, P., Edavazhippurath, A., Dhanasooraj, D., Puthenpurayil, J.M., Chakkiyar, K., Mishra, A., Batra, A., Punnen, A., Kumar, S., Sivasubbu, S. & Scaria, V. Spectrum of clinical features and genetic variants in mevalonate kinase (MVK) gene of South Indian families suffering from Hyperimmunoglobulin D Syndrome. *PLoS One* **15**, e0237999 (2020).
35. Koelsch, K., Zheng, N.Y., Zhang, Q., Duty, A., Helms, C., Mathias, M.D., Jared, M., Smith, K., Capra, J.D. & Wilson, P.C. Mature B cells class switched to IgD are autoreactive in healthy individuals. *J Clin Invest* **117**, 1558-1565 (2007).
36. Rijkers, T., Van Den Ouweland, J., Morolli, B., Rolink, A.G., Baarends, W.M., Van Sloun, P.P., Lohman, P.H. & Pastink, A. Targeted inactivation of mouse RAD52 reduces homologous recombination but not resistance to ionizing radiation. *Mol Cell Biol* **18**, 6423-6429 (1998).
37. Sung, P. Function of yeast Rad52 protein as a mediator between replication protein A and the Rad51 recombinase. *J Biol Chem* **272**, 28194-28197 (1997).
38. Symington, L.S., Rothstein, R. & Lisby, M. Mechanisms and regulation of mitotic recombination in Saccharomyces cerevisiae. *Genetics* **198**, 795-835 (2014).
39. Song, B. & Sung, P. Functional interactions among yeast Rad51 recombinase, Rad52 mediator, and replication protein A in DNA strand exchange. *J Biol Chem* **275**, 15895-15904 (2000).
40. Sung, P., Trujillo, K.M. & Van Komen, S. Recombination factors of Saccharomyces cerevisiae. *Mutat Res* **451**, 257-275 (2000).
41. Seong, C., Colavito, S., Kwon, Y., Sung, P. & Krejci, L. Regulation of Rad51 recombinase presynaptic filament assembly via interactions with the Rad52 mediator and the Srs2 anti-recombinase. *J Biol Chem* **284**, 24363-24371 (2009).
42. Wilson, P.F., Hinz, J.M., Urbin, S.S., Nham, P.B. & Thompson, L.H. Influence of homologous recombinational repair on cell survival and chromosomal aberration induction during the cell cycle in gamma-irradiated CHO cells. *DNA Repair* **9**, 737-744 (2010).

43. Du, L.Q., Wang, Y., Wang, H., Cao, J., Liu, Q. & Fan, F.Y. Knockdown of Rad51 expression induces radiation- and chemo-sensitivity in osteosarcoma cells. *Med Oncol* **28**, 1481-1487 (2011).
44. Thorslund, T., McIlwraith, M.J., Compton, S.A., Lekomtsev, S., Petronczki, M., Griffith, J.D. & West, S.C. The breast cancer tumor suppressor BRCA2 promotes the specific targeting of RAD51 to single-stranded DNA. *Nat Struct Mol Biol* **17**, 1263-1265 (2010).
45. Kwon, Y. & Sung, P. Rad52, maestro of inverse strand exchange. *Mol Cell* **67**, 1-3 (2017).
46. Feng, Z., Scott, S.P., Bussen, W., Sharma, G.G., Guo, G., Pandita, T.K. & Powell, S.N. Rad52 inactivation is synthetically lethal with BRCA2 deficiency. *Proc Natl Acad Sci U S A* **108**, 686-691 (2011).
47. Ma, C.J., Kwon, Y., Sung, P. & Greene, E.C. Human RAD52 interactions with replication protein A and the RAD51 presynaptic complex. *J Biol Chem* **292**, 11702-11713 (2017).
48. Symington, L.S. Role of RAD52 epistasis group genes in homologous recombination and double-strand break repair. *Microbiol Mol Biol Rev* **66**, 630-670 (2002).
49. Ciccia, A. & Symington, L.S. Stressing Out About RAD52. *Mol Cell* **64**, 1017-1019 (2016).
50. Truong, L.N., Li, Y., Shi, L.Z., Hwang, P.Y., He, J., Wang, H., Razavian, N., Berns, M.W. & Wu, X. Microhomology-mediated End Joining and Homologous Recombination share the initial end resection step to repair DNA double-strand breaks in mammalian cells. *Proc Natl Acad Sci U S A* **110**, 7720-7725 (2013).
51. Abayasingam, A., Balachandran, H., Agapiou, D., Hammoud, M., Rodrigo, C., Keoshkerian, E., Li, H., Brasher, N.A., Christ, D., Rouet, R., Burnet, D., Grubor-Bauk, B., Rawlinson, W., Turville, S., Aggarwal, A., Stella, A.O., Fichter, C., Brilot, F., Mina, M., Post, J.J., Hudson, B., Gilroy, N., Dwyer, D., Sasson, S.C., Tea, F., Pilli, D., Kelleher, A., Tedla, N., Lloyd, A.R., Martinello, M., Bull, R.A. & Group, C.S. Long-term persistence of RBD(+) memory B cells encoding neutralizing antibodies in SARS-CoV-2 infection. *Cell Rep Med* **2**, 100228 (2021).
52. Waters, L.R., Ahsan, F.M., Ten Hoeve, J., Hong, J.S., Kim, D.N.H., Minasyan, A., Braas, D., Graeber, T.G., Zangle, T.A. & Teitell, M.A. Ampk regulates IgD expression but not energy stress with B cell activation. *Sci Rep* **9**, 8176 (2019).
53. Sag, D., Carling, D., Stout, R.D. & Suttles, J. Adenosine 5'-monophosphate-activated protein kinase promotes macrophage polarization to an anti-inflammatory functional phenotype. *J Immunol* **181**, 8633-8641 (2008).
54. Moskophidis, D., Moskophidis, M. & Lohler, J. Virus-specific IgD in acute viral infection of mice. *J Immunol* **158**, 1254-1261 (1997).
55. Forsgren, A., Brant, M., Mollenkvist, A., Muyombwe, A., Janson, H., Woin, N. & Riesbeck, K. Isolation and characterization of a novel IgD-binding protein from Moraxella catarrhalis. *J Immunol* **167**, 2112-2120 (2001).
56. Min, J.Y., Nayak, J.V., Hulse, K.E., Stevens, W.W., Raju, P.A., Huang, J.H., Suh, L.A., Van Roey, G.A., Norton, J.E., Carter, R.G., Price, C.P.E., Weibman, A.R., Rashan, A.R., Ghosn, E.E., Patel, Z.M., Homma, T., Conley, D.B., Welch, K.C., Shintani-Smith, S., Peters, A.T., Grammer, L.C., 3rd, Harris, K.E., Kato, A., Hwang, P.H., Kern, R.C., Herzenberg, L.A., Schleimer, R.P. & Tan, B.K. Evidence for altered levels of IgD in the nasal airway mucosa of patients with chronic rhinosinusitis. *J Allergy Clin Immunol* **140**, 1562-1571 (2017).
57. Casali, P. & Notkins, A.L. Probing the human B-cell repertoire with EBV: polyreactive antibodies and CD5+ B lymphocytes. *Annu Rev Immunol* **7**, 513-535 (1989).
58. Ikematsu, H., Kasaian, M.T., Schettino, E.W. & Casali, P. Structural analysis of the VH-D-JH segments of human polyreactive IgG mAb. Evidence for somatic selection. *J Immunol* **151**, 3604-3616 (1993).
59. Ichiyoshi, Y. & Casali, P. Analysis of the structural correlates for antibody polyreactivity by multiple reassortments of chimeric human immunoglobulin heavy and light chain V segments. *J Exp Med* **180**, 885-895 (1994).
60. Casali, P. & Schettino, E.W. Structure and function of natural antibodies. *Curr Top Microbiol Immunol* **210**, 167-179 (1996).
61. Sabouri, Z., Perotti, S., Spierings, E., Humburg, P., Yabas, M., Bergmann, H., Horikawa, K., Roots, C., Lambe, S., Young, C., Andrews, T.D., Field, M., Enders, A., Reed, J.H. & Goodnow, C.C. IgD attenuates the IgM-induced anergy response in transitional and mature B cells. *Nat Commun* **7**, 13381 (2016).
62. Guo, L., Tian, J., Guo, Z., Zheng, B. & Han, S. The absence of immunoglobulin D B cell receptor-mediated signals promotes the production of autoantibodies and exacerbates glomerulonephritis in murine lupus. *Clin Exp Immunol* **164**, 227-235 (2011).
63. Houten, S.M., Kuis, W., Duran, M., de Koning, T.J., van Royen-Kerkhof, A., Romeijn, G.J., Frenkel, J., Dorland, L., de Barse, M.M., Huijbers, W.A., Rijkers, G.T., Waterham, H.R., Wanders, R.J. & Poll-The, B.T. Mutations in MVK, encoding mevalonate kinase, cause hyperimmunoglobulinaemia D and periodic fever syndrome. *Nat Genet* **22**, 175-177 (1999).

969 64. Muramatsu, M., Kinoshita, K., Fagarasan, S., Yamada, S., Shinkai, Y. & Honjo, T. Class switch recombination and
970 hypermutation require activation-induced cytidine deaminase (AID), a potential RNA editing enzyme. *Cell* **102**, 553-
971 563 (2000).

972 65. Park, S.-R., Zan, H., Zhang, J., Al-Qahtani, A., Pone, E.J., Xu, Z., Mai, T. & Casali, P. HoxC4 binds to the promoter of
973 the cytidine deaminase AID gene to induce AID expression, class-switch DNA recombination and somatic
974 hypermutation. *Nat Immunol* **10**, 540-550 (2009).

975 66. White, C.A., Pone, E.J., Lam, T., Tat, C., Hayama, K.L., Li, G., Zan, H. & Casali, P. Histone deacetylase inhibitors
976 upregulate B cell microRNAs that silence AID and Blimp-1 expression for epigenetic modulation of antibody and
977 autoantibody responses. *J Immunol* **193**, 5933-5950 (2014).

978 67. Zan, H., Zhang, J., Al-Qahtani, A., Pone, E.J., White, C.A., Lee, D., Yel, L., Mai, T. & Casali, P. Endonuclease G plays
979 a role in immunoglobulin class switch DNA recombination by introducing double-strand breaks in switch regions. *Mol*
980 *Immunol* **48**, 610-622 (2011).

981 68. Xu, Z., Fulop, Z., Wu, G., Pone, E.J., Zhang, J., Mai, T., Thomas, L.M., Al-Qahtani, A., White, C.A., Park, S.R.,
982 Steinacker, P., Li, Z., Yates, J., 3rd, Herron, B., Otto, M., Zan, H., Fu, H. & Casali, P. 14-3-3 adaptor proteins recruit
983 AID to 5'-AGCT-3'-rich switch regions for class switch recombination. *Nat Struct Mol Biol* **17**, 1124-1135 (2010).

984 69. Zan, H., White, C.A., Thomas, L.M., Mai, T., Li, G., Xu, Z., Zhang, J. & Casali, P. Rev1 recruits Ung to switch regions
985 and enhances dU glycosylation for immunoglobulin class switch DNA recombination. *Cell Rep* **2**, 1220-1232 (2012).

986 70. Li, G., White, C.A., Lam, T., Pone, E.J., Tran, D.C., Hayama, K.L., Zan, H., Xu, Z. & Casali, P. Combinatorial
987 H3K9acS10ph histone modification in IgH locus S regions targets 14-3-3 adaptors and AID to specify antibody class-
988 switch DNA recombination. *Cell Rep* **5**, 702-714 (2013).

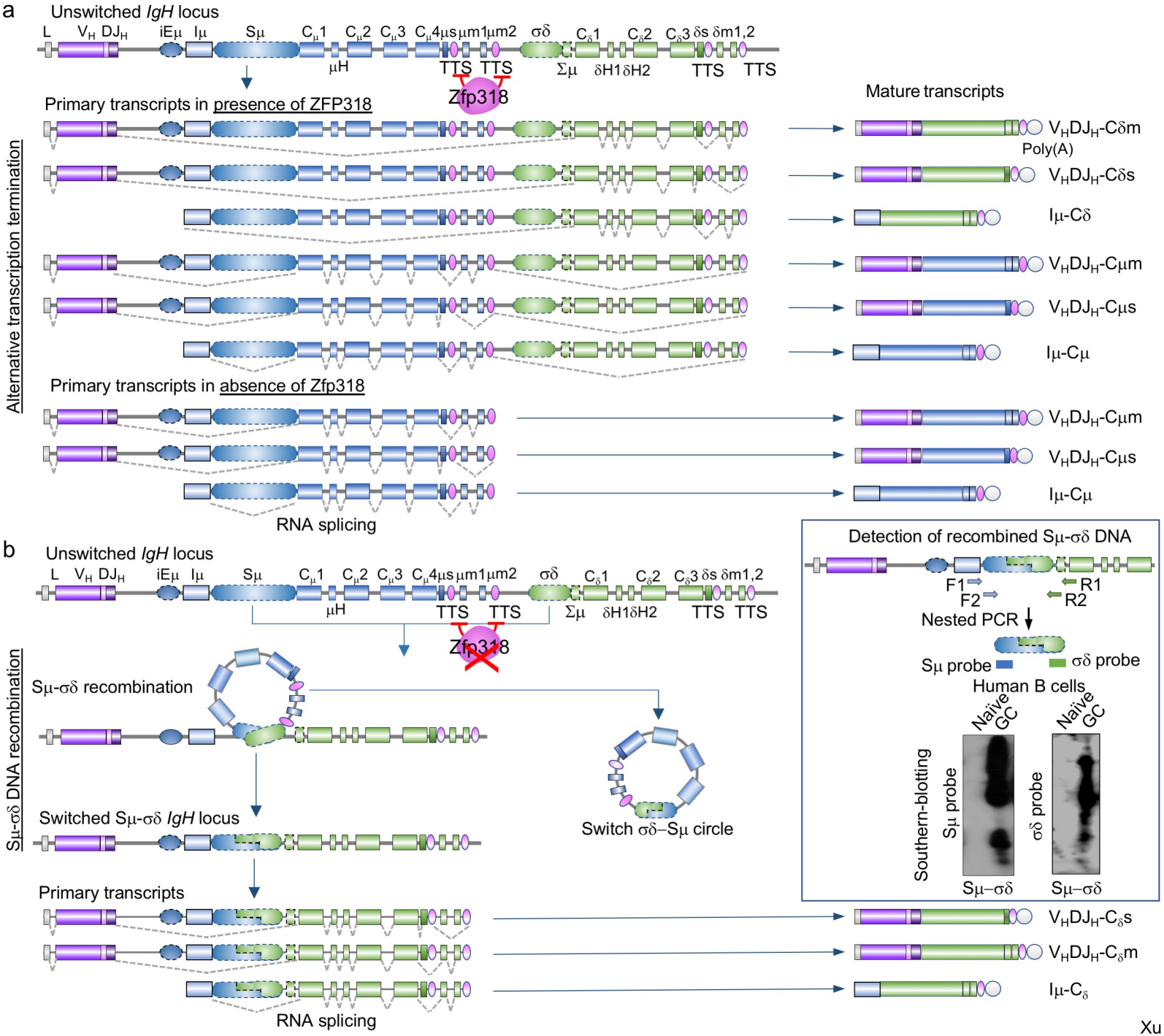

Xu et al., Figure 1

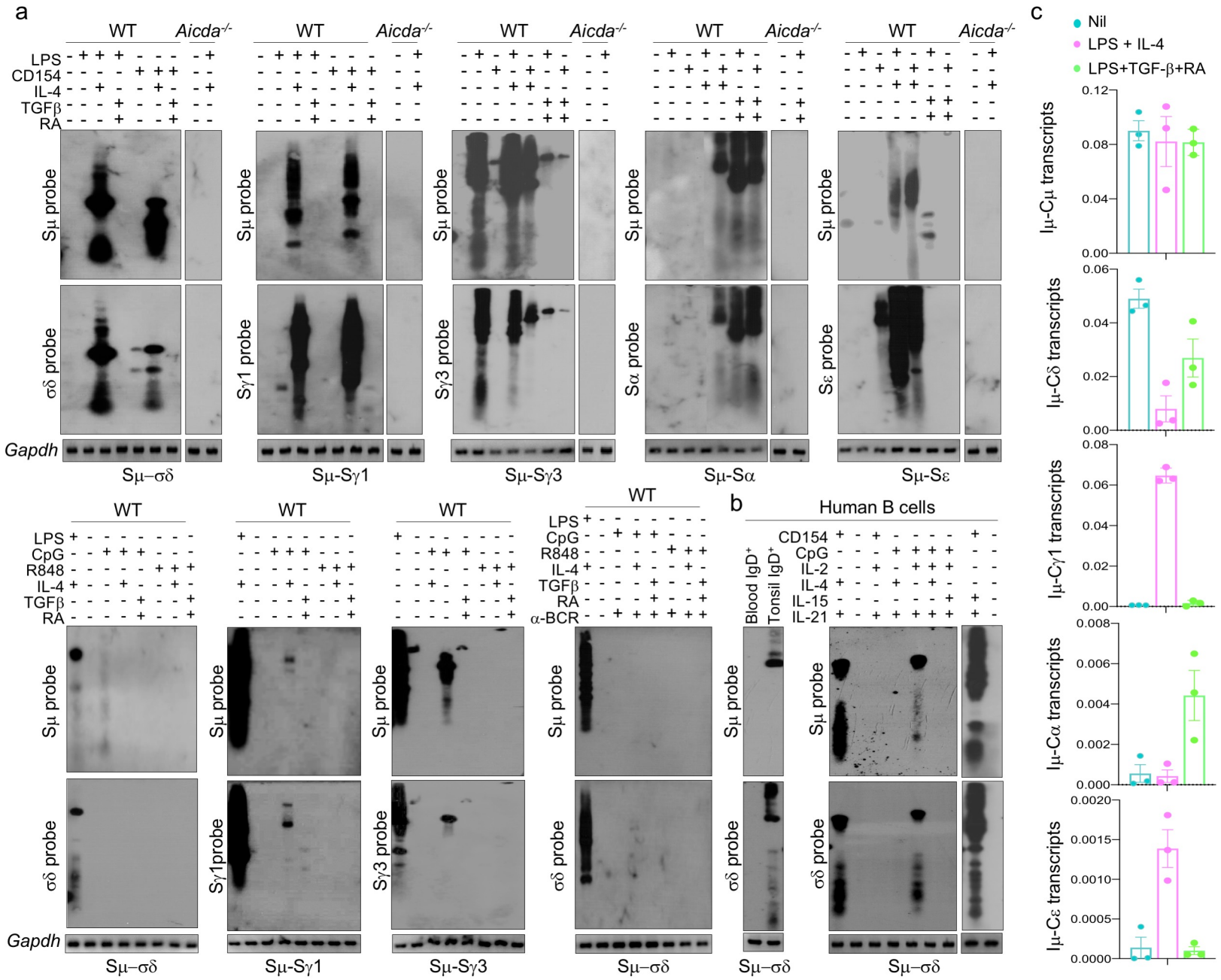

Xu et al., Figure 2

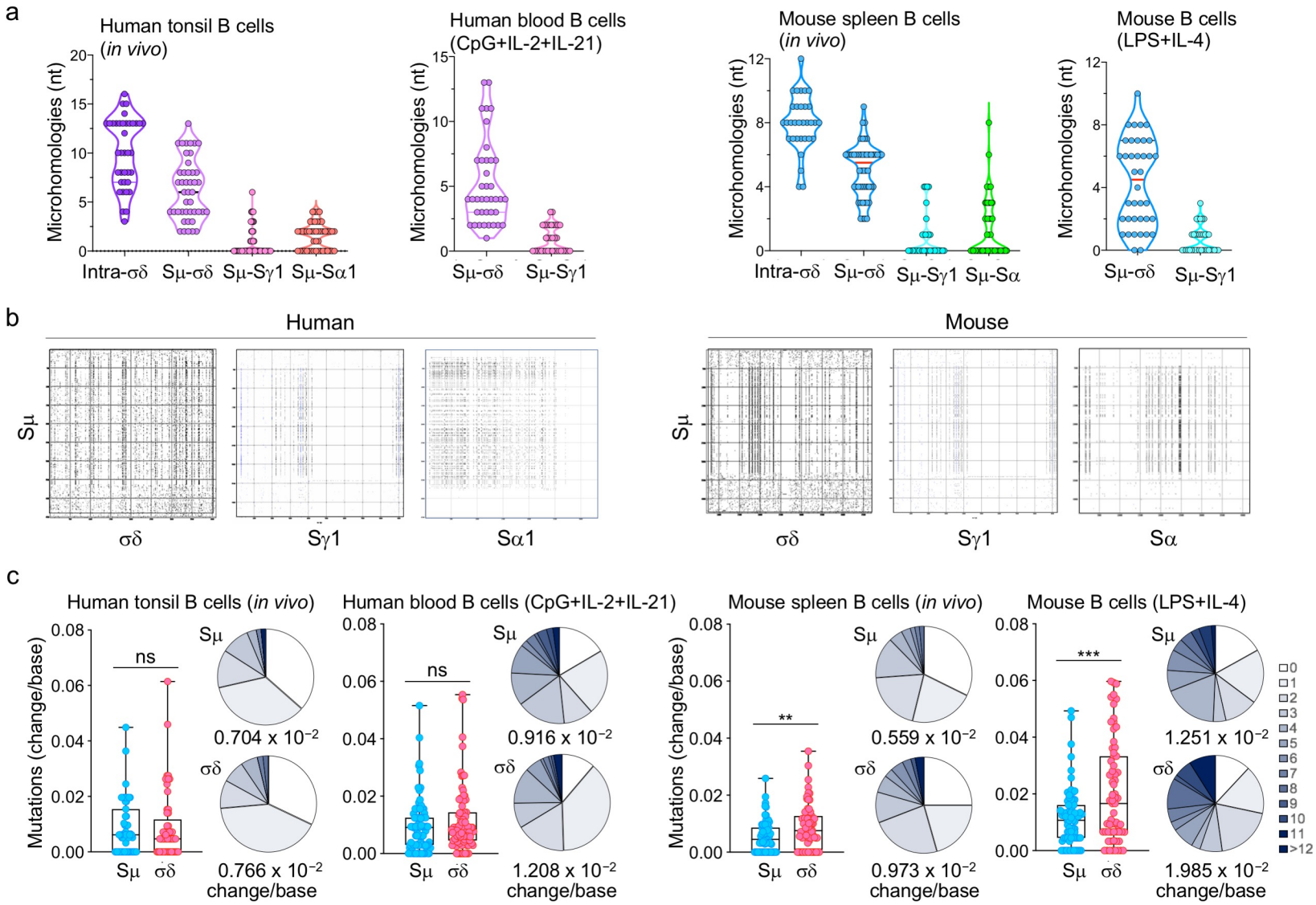

Xu et al., Figure 3

Human tonsil B cells (*in vivo*)

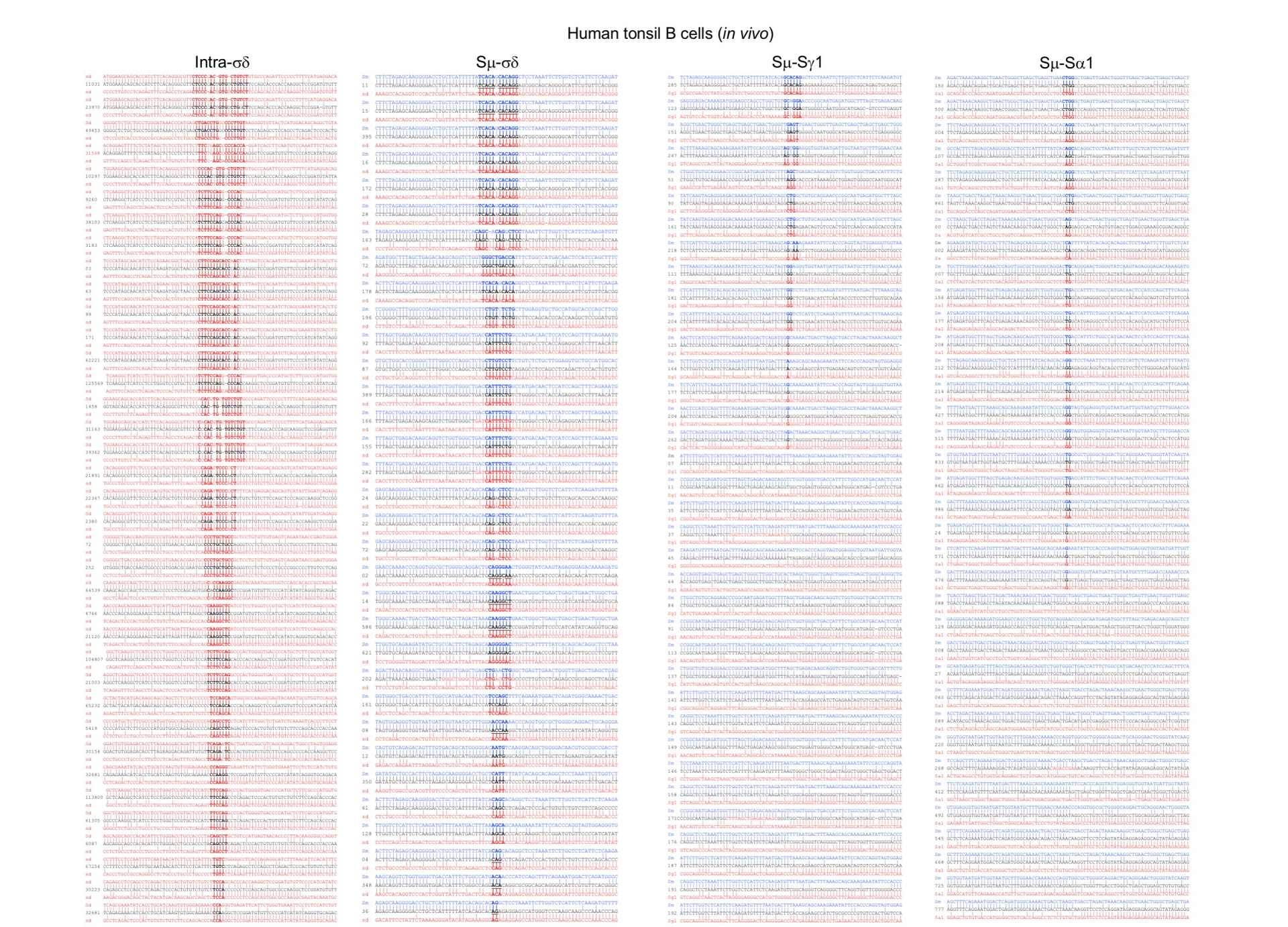

Xu et al., Figure 4

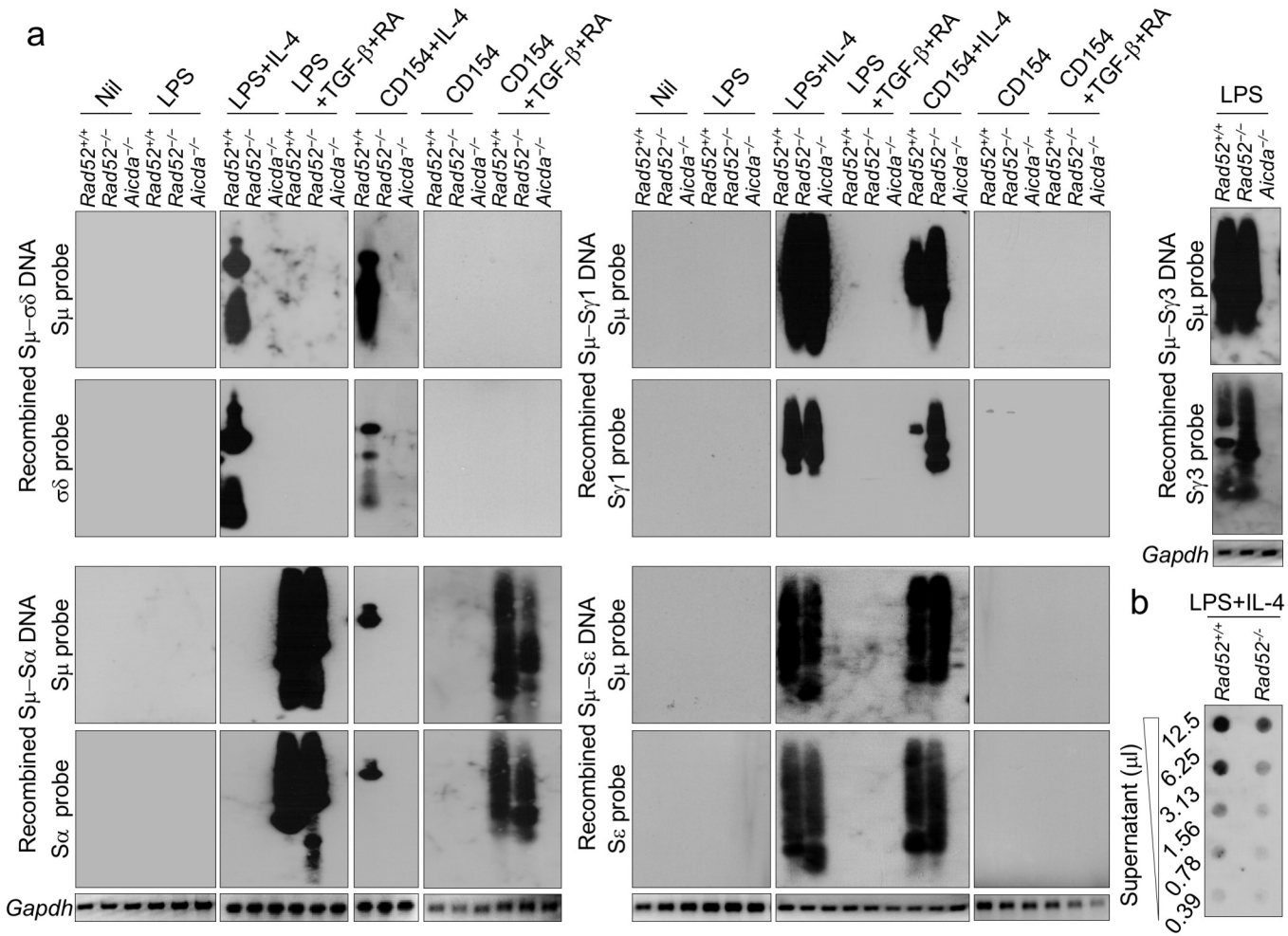

Xu et al., Figure 5

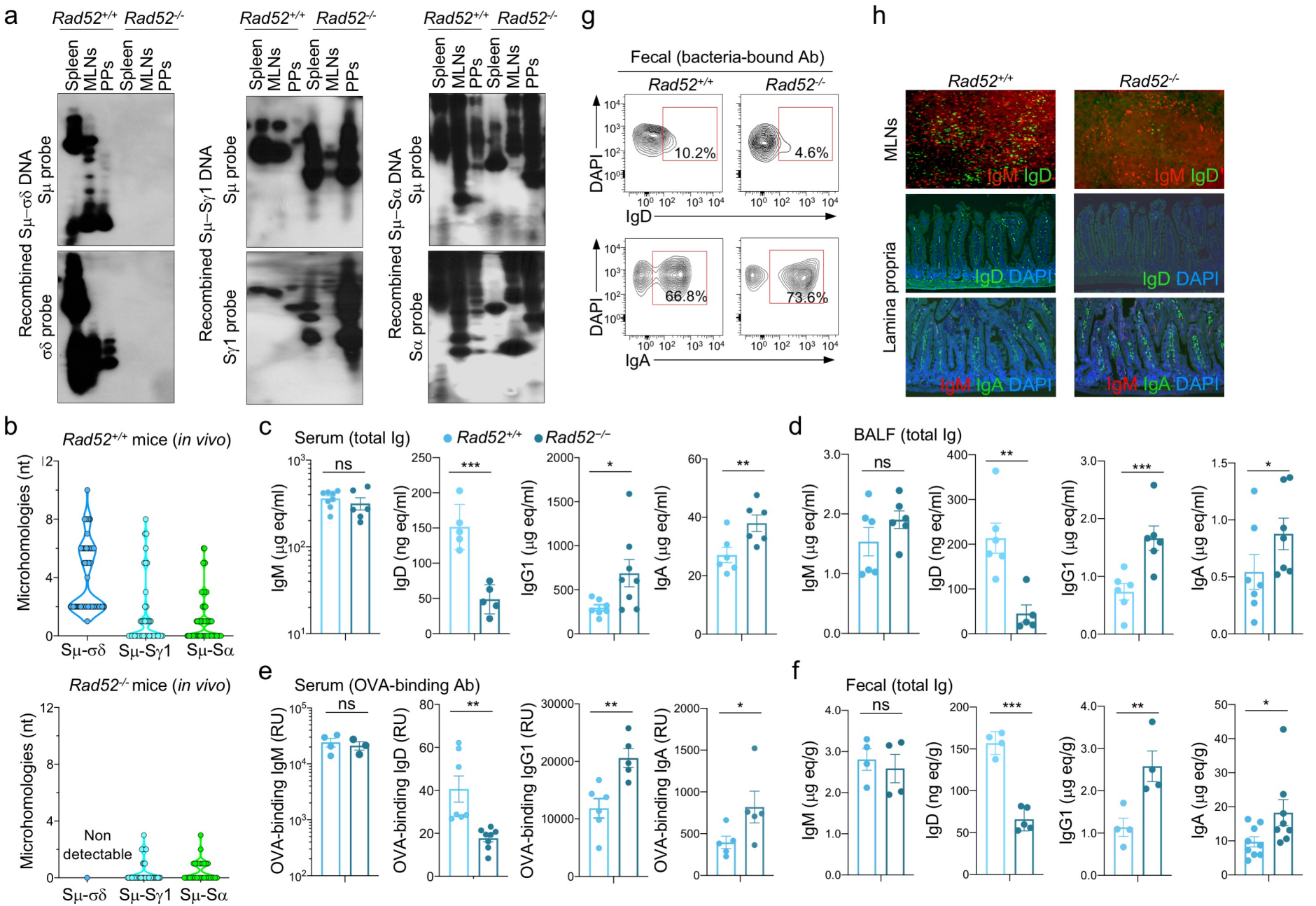

Xu et al., Figure 6

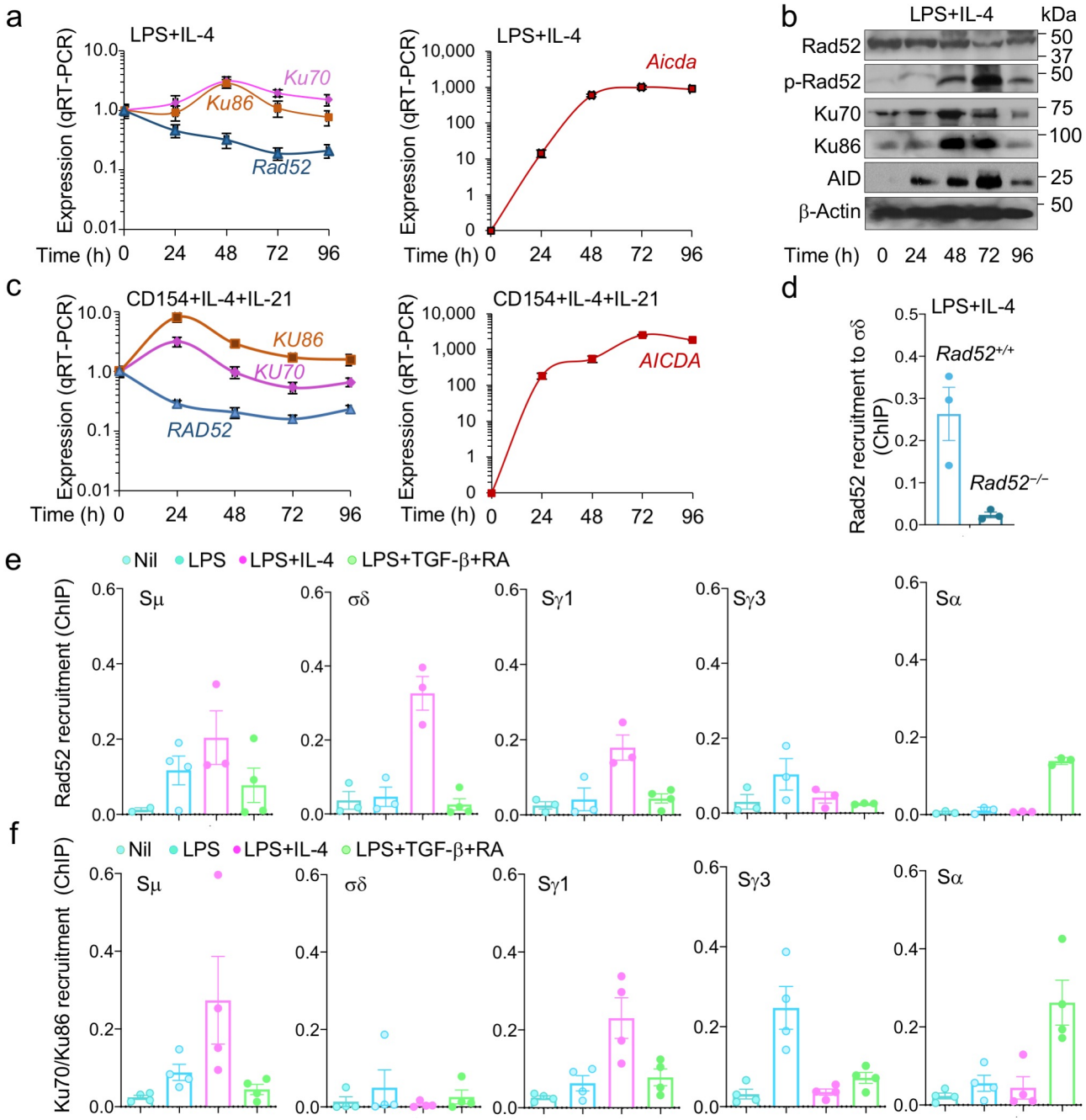

Xu et al., Figure 7

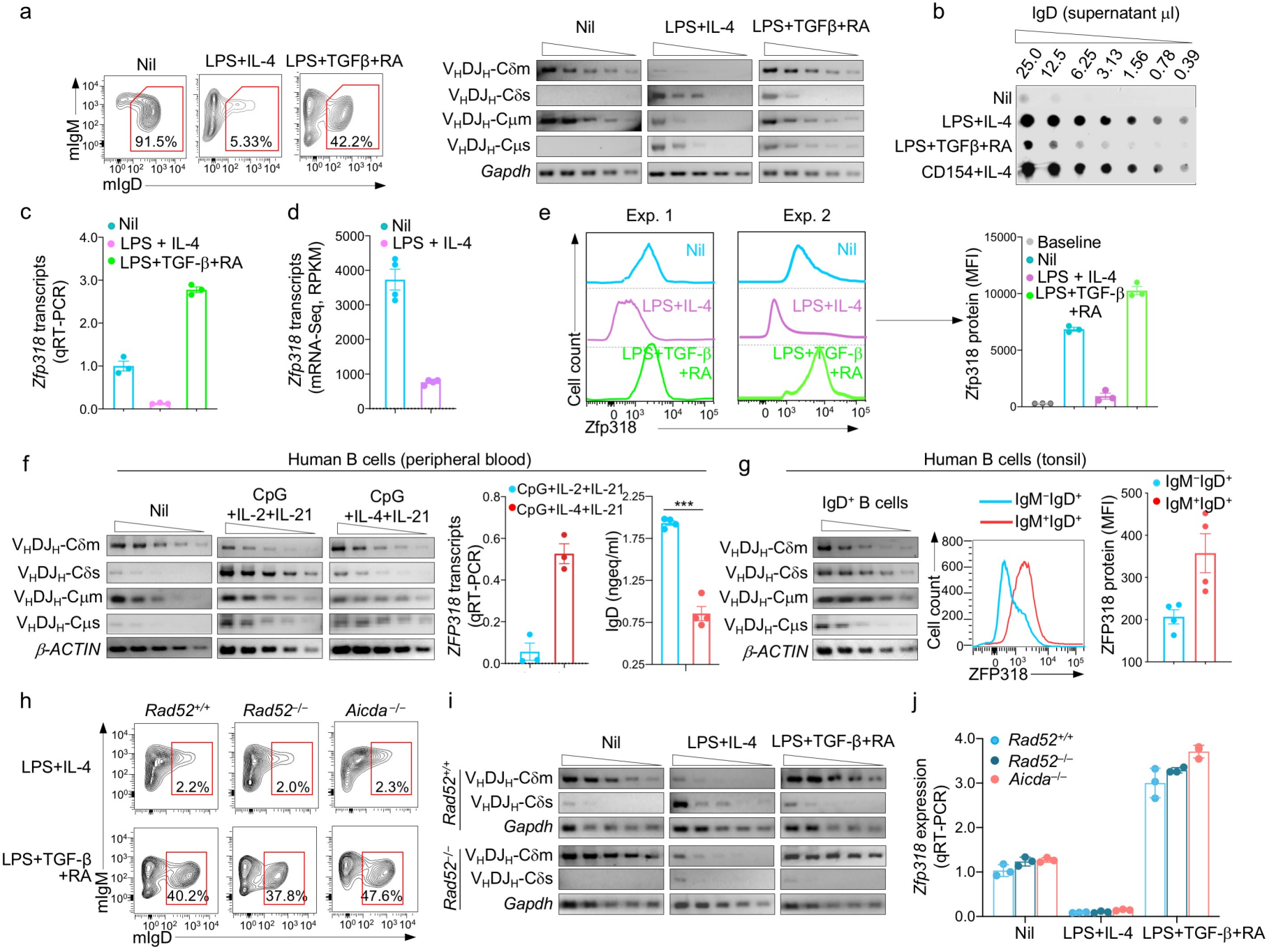

Xu et al., Figure 8

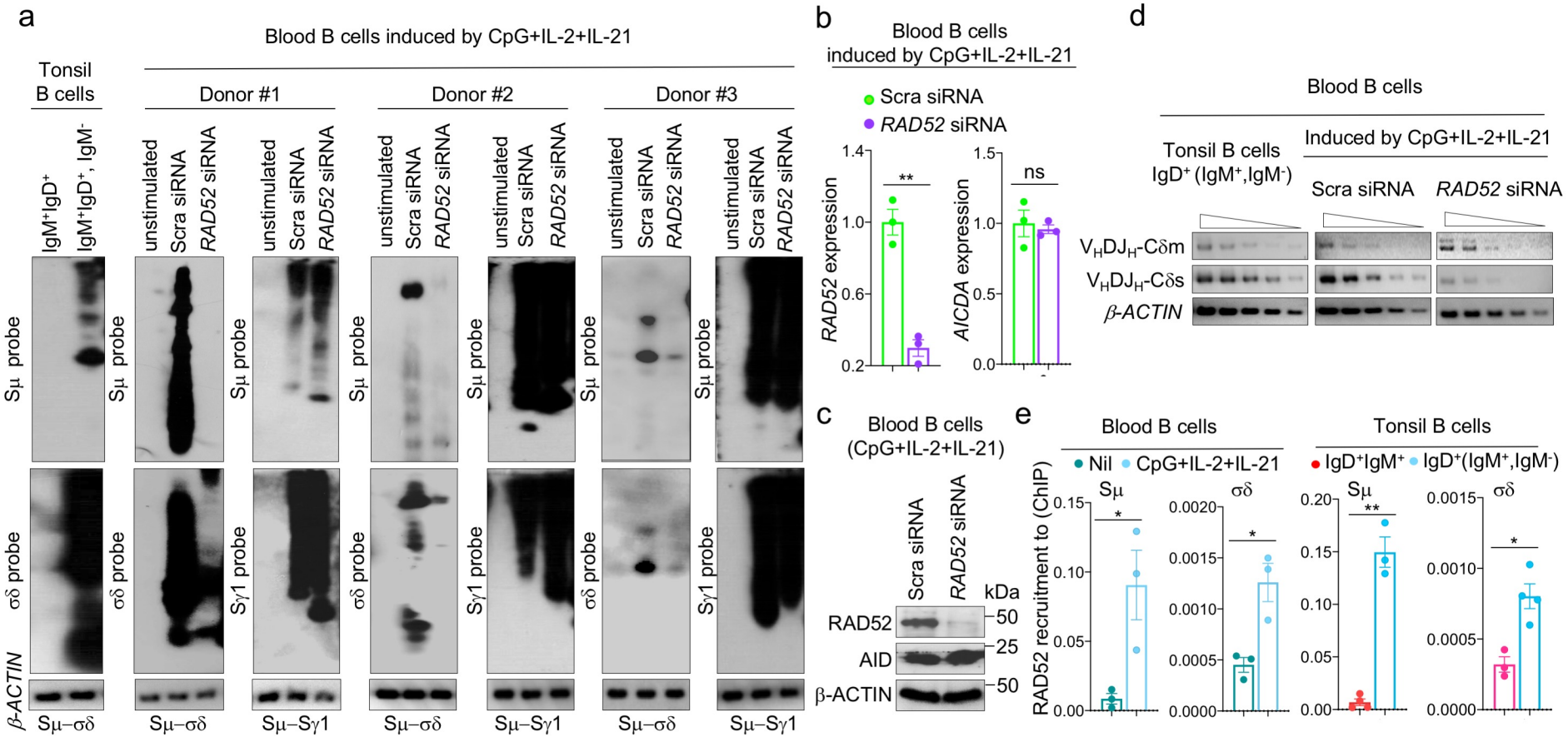

Xu et al., Figure 9

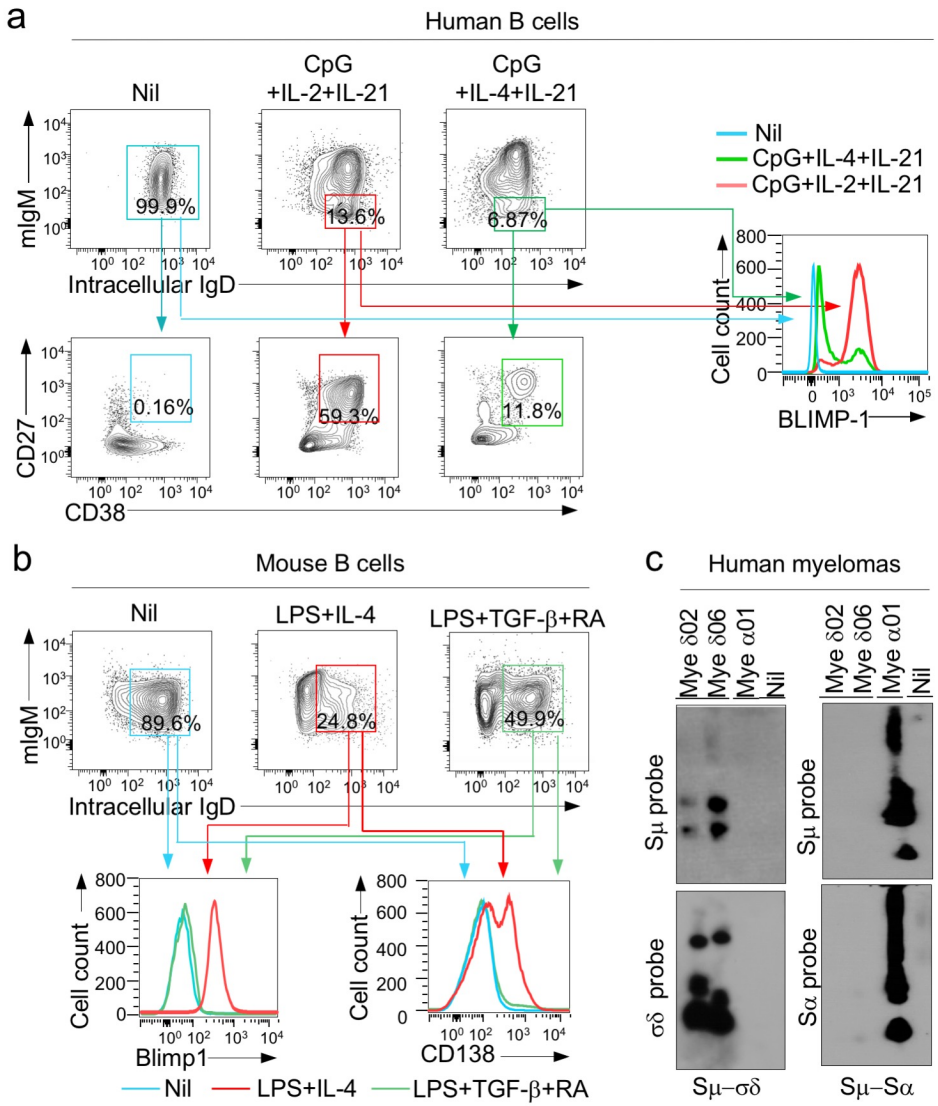

Xu et al., Figure 10

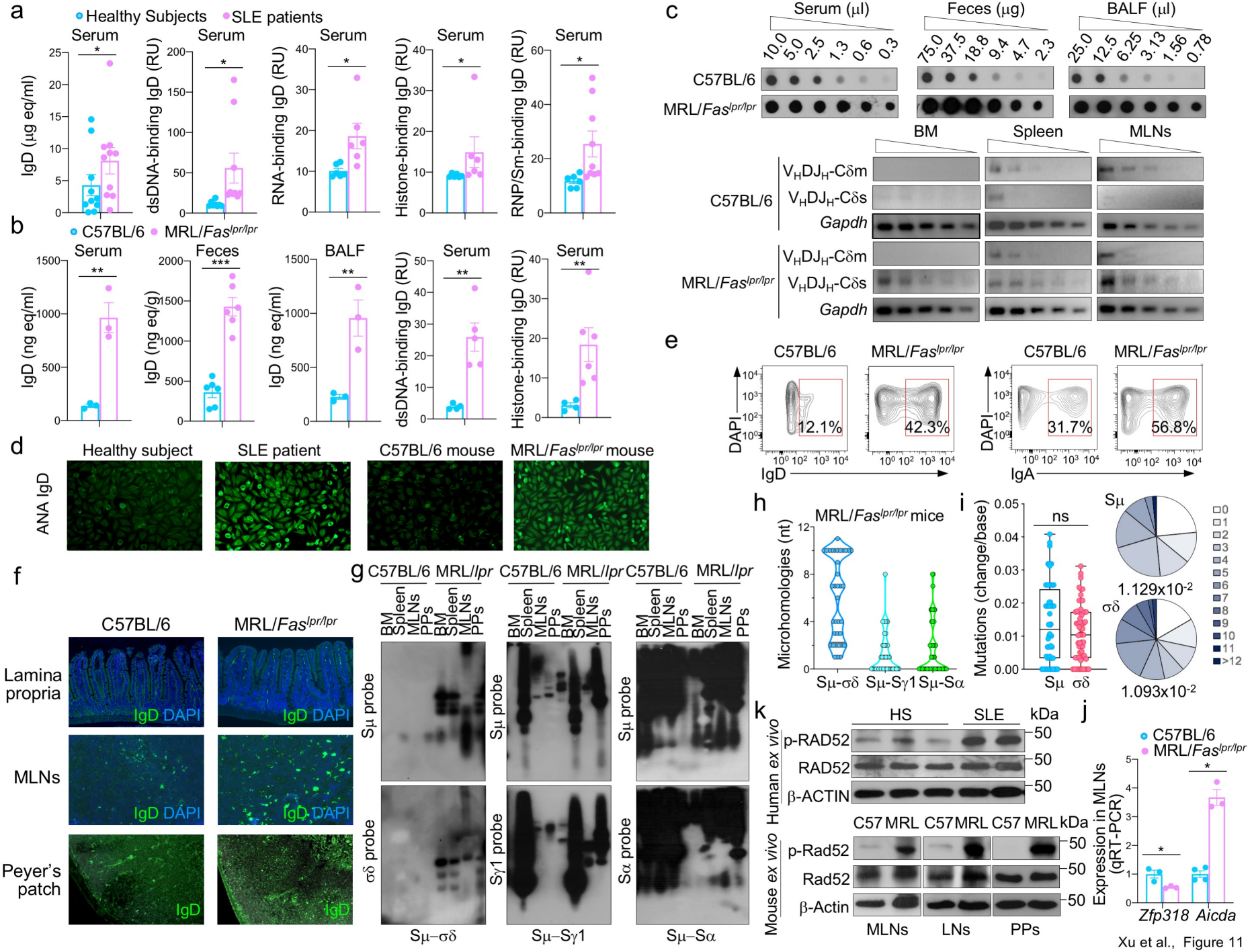

Xu et al., Figure 11